AN INVESTIGATION OF ELECTRO-OPTICAL TURBULENCE PARAMETERS

Valente Macias

NAVAL POSTGRADUATE SCHOOL
Monterey, California

THESIS

AN INVESTIGATION OF ELECTRO-

OPTICAL TURBULENCE PARAMETERS

by

Valente Macias, Jr.

June 1977

Thesis Advisor: K. L. Davidson

SECURITY CLASSIFICATION OF THIS PAGE (When Data Entered)

REPORT DOCUMENTATION PAGE

READ INSTRUCTIONS BEFORE COMPLETING FORM

1. REPORT NUMBER	2. GOVT ACCESSION NO. / 3. RECIPIENT'S CATALOG NUMBER
4. TITLE (and Subtitle): An Investigation of Electro-Optical Turbulence Parameters	5. TYPE OF REPORT & PERIOD COVERED: Master's Thesis; June 1977
	6. PERFORMING ORG. REPORT NUMBER
7. AUTHOR(s): Valente Macias, Jr.	8. CONTRACT OR GRANT NUMBER(s)
9. PERFORMING ORGANIZATION NAME AND ADDRESS: Naval Postgraduate School, Monterey, California 93940	10. PROGRAM ELEMENT, PROJECT, TASK AREA & WORK UNIT NUMBERS
11. CONTROLLING OFFICE NAME AND ADDRESS: Naval Postgraduate School, Monterey, California 93940	12. REPORT DATE: June 1977
	13. NUMBER OF PAGES: 68
14. MONITORING AGENCY NAME & ADDRESS(if different from Controlling Office): Naval Postgraduate School, Monterey, California 93940	15. SECURITY CLASS. (of this report): Unclassified
	15a. DECLASSIFICATION/DOWNGRADING SCHEDULE

16. DISTRIBUTION STATEMENT (of this Report)

Approved for public release; distribution unlimited.

17. DISTRIBUTION STATEMENT (of the abstract entered in Block 20, if different from Report)

18. SUPPLEMENTARY NOTES

19. KEY WORDS (Continue on reverse side if necessary and identify by block number)

20. ABSTRACT (Continue on reverse side if necessary and identify by block number)

Mean humidity, temperature, wind data and fluctuating temperature and velocities data obtained from the R/V Acania were interpreted on the basis of empirically derived expressions describing the temperature structure parameter, C_T^2, and the dissipation rate of turbulent kinetic energy, ε. Properties of C_T^2 and ε are related to a stability parameter Z/L and the Richardson number, Ri. Non-dimensional temperature

DD FORM 1 JAN 73 1473 EDITION OF 1 NOV 65 IS OBSOLETE
S/N 0102-014-6601 |

SECURITY CLASSIFICATION OF THIS PAGE (When Data Entered)

structure functions parameters, $C_T^2/Z^{4/3}(\partial\theta/\partial z)^2$, and turbulent kinetic energy dissipation rates, $K\varepsilon\ ZU_*^{-3}$, versus Ri were examined for open ocean conditions.

This experiment verified earlier hypotheses that the profiles obtained from empirically derived expressions using overwater data are very much different from those obtained using overland data. The distribution of the non-dimensional turbulent kinetic energy dissipation rate agreed with that predicted by similarity theory.

An Investigation of Electro-Optical Turbulence Parameters

by

Valente Macias, Jr.
Captain, United States Air Force
B.S., Florida State University, 1969

Submitted in partial fulfillment of the
requirements for the degree of

MASTER OF SCIENCE IN METEOROLOGY

from the

NAVAL POSTGRADUATE SCHOOL
June 1977

ABSTRACT

Mean humidity, temperature, wind data and fluctuating temperature and velocities data obtained from the R/V Acania were interpreted on the basis of empirically derived expressions describing the temperature structure parameter, C_T^2, and the dissipation rate of turbulent kinetic energy, ε . Properties of C_T^2 and ε are related to a stability parameter Z/L and the Richardson number, Ri. Non-dimensional temperature structure functions parameters, $C_T^2/Z^{4/3}(\frac{\partial\theta}{\partial z})^2$, and turbulent kinetic energy dissipation rates, $K\varepsilon\ ZU_*^{-3}$, versus Ri were examined for open ocean conditions.

This experiment verified earlier hypotheses that the profiles obtained from empirically derived expressions using overwater data are very much different from those obtained using overland data. The distribution of the non-dimensional turbulent kinetic energy dissipation rate agreed with that predicted by similarity theory.

TABLE OF CONTENTS

LIST OF FIGURES

LIST OF SYMBOLS AND ABBREVIATIONS

C_n	Refractive index-structure parameter
C_T	Temperature index-structure parameter
ρ	Density
ε	Rate of dissipation of turbulent kinetic energy
F	Buoyancy force
f	Temporal frequency
g	Acceleration due to gravity
k	Wave number
κ	von Karmon constant, 0.35
ℓ	Local mixing length
L_o	Lower limit of the inertial subrange (micro-scale)
ℓ_o	Upper limit of the inertial subrange (micro-scale)
x	Rate of dissipation of temperature variance
n	Refractive index
P	Ambient pressure
$\bar{q}$	Mean specific humidity, g/kg
q_*	$= -\overline{w'q'}/U_*$
r	Separation distance in defining structure function
Ri	Richardson number
u',v',w'	Velocity fluctuations (along wind, crosswind and vertical components)
$S_T(k)$	Temperature variance spectral density
T	Ambient temperature
$\bar{T}$	Mean temperature

T_*	Scaling temperature, $(-\overline{w'T'}/U_*)$
T_{*_v}	Scaling virtual temperature, $T_* + 0.61q_*\bar{T}$
$\bar{U}$	Mean horizontal wind speed
U_*	Friction velocity, $(-\overline{U'w'})^{\frac{1}{2}}$
z	Height
Z/L	Stability parameter ratio of height to the Monin-Obukhov length

SYMBOLS USED IN BULK AERODYNAMIC FORMULAE

$\bar{U}$ = average wind speed at height z, m/z

T_a = average potential air temperature at height h, K

Q_a = average water vapor density at height z, g/m^3

T_s = average sea surface temperature

Q_s = average water vapor density adjacent to the sea surface usually obtained by assuming the air to be saturated, i.e., at dew point T_s, g/m^3

C_D = drag coefficient, from experiment

C_H = sensible heat flux coefficient, from experiment

C_E = moisture flux coefficient, from experiment

z = reference height, usually 10 m above the average sea surface

w' = vertical velocity fluctuation, m/s

q' = moisture fluctuation, g/m^3

θ = potential temperature fluctuation, K

ACKNOWLEDGEMENTS

I would like to express my sincere gratitude to Professor Kenneth Davidson, without whose expert advice, this project may not have been finished. My utmost thanks go to Professor Tom Houlihan, Dr. Chris Fairall, and Dr. Gordon Schacher, whose expertise on instrumentation and evaluation of data kept me on the proper path and saved me numerous man hours in interpretation of data for this study.

My fondest gratitude is expressed to my wife, Meme, and three boys, Marcos, Damian, and Gabriel. Without their constant expression of faith in me and their never ending encouragement and patience, none of this would have been possible or worthwhile.

I. INTRODUCTION

The marine boundary layer is that region in the first kilometer over the sea which is defined principally by turbulent transfer of momentum and heat. In the past decade there have been concentrated efforts to make measurements in this region and to define physical expressions describing the turbulent intensities. The marine environment presents a number of problems, especially in accessibility, platform stability, and sensor protection. Most important of these problems are the lack of an extensive data bases and the fact that available turbulence expressions, which are empirical in nature, have been formulated primarily from overland data.

With the development of systems dependent on laser technology, the Department of Defense interest in turbulence in this region pertains to assessing and predicting the environmental influence on optical wave propagation. The refractive index problem for the marine boundary layer is more complicated than the similar problem over land because of the difficulties in making point measurements of the fluctuating air temperature from which refractive index statistics for optical waves are often obtained. For optical waves the atmospheric index of refraction variations primary result from temperature-induced density changes. These variations cause scintillation and phase fluctuations of laser beams propagated in the

atmosphere and the loss of sight of objects viewed through high magnification telescopes.

An interdisciplinary group at the Naval Postgraduate School has been involved in overwater experiments to relate the optical properties and the optically relevant meteorological parameters of the marine boundary layer to observable bulk atmospheric parameters.

The primary purpose of this work was to evaluate previously formulated overland expressions for the overwater regime. Expressions presented by Wyngaard et al. (1971) and Friehe (1976) were used to relate C_T^2 to a stability parameter, either the Richardson number or Z/L where L is Monin-Obukhov Length. In addition to this, expressions described by Busch and Panofsky (1968) were used to relate ε to the stability parameters.

Ten minute time averaged values of wind, temperature, and relative humidity measured at four levels (4.2, 6.6, 11.3, and 17.7 meters) were examined in this study. The most recent and the majority of the observations examined were made during the months of September and October 1976 off the coast of San Diego, California. Data previously evaluated by Hughes (1976) and Karach (1976) were incorporated into the final evaluations to supplement the data base. The latter data were also measured at four levels (4.2, 6.6, 7.6, and 13.9 meters).

II. THEORETICAL BACKGROUND

A. GENERAL

C_T^2 and ε are optically relevant turbulence parameters because they define the intensity of fluctuations in the refractive index and the size or scale of refractive index inhomogeneities, respectively. The scales of the temperature inhomogeneities that distort image resolution and degrade laser beam propagation in the atmospheric surface layer lie in the inertial subrange where fluctuations are isotropic.

The latter characteristic allows theories by Tatarski (1961) describing electromagnetic propagation to be applied in analyses. Tatarski considered the refractive-index-structure parameter,

$$C_n^2 = \frac{\overline{[n(x) - n(x+r)]}^2}{r^{2/3}} \qquad (1)$$

which is related to the temperature structure function parameter, C_T^2, as

$$C_T^2 = (79 \times 10^{-6} \frac{P}{T^2})^{-2} C_n^2 \qquad (2)$$

where P is the pressure and T the temperature of the atmosphere. C_T^2 may be evaluated in a number of methods.

The dissipation rate ε defines the micro-scale, ℓ_o, as

$$\ell_o = (\frac{\gamma^3}{\varepsilon})^{\frac{1}{4}} \qquad (3)$$

where γ is the kinematic molecular viscosity. The micro-scale appears in optical parameters for image resolution. For example, the exp(-2) folding distance of the mutual coherence, ρ_o is defined as

$$\rho_o = \frac{1}{(1.5C_n \ell_o^{-1/6} \bar{K})} \tag{4}$$

where $\bar{K}$ is the average wave number.

B. TEMPERATURE STRUCTURE-FUNCTION PARAMETER, C_T^2

The temperature structure-function parameter may be evaluated or estimated by several different methods depending on the measurement procedures. At separations r of the order of inertial subrange scales, the temperature structure-function in a locally isotropic field has the form

$$C_T^2 = \frac{\langle [T(x) - T(x+r)]^2 \rangle}{r^{2/3}} \tag{5}$$

C_T^2 can also be related to the one-dimensional temperature spectrum (The Fourier transform of the correlation function with separations in the streamwise direction) in the inertial subrange as

$$S_T(K_1) = .25\ C_T^2\ K_1^{-5/3} \tag{6}$$

K_1 is the streamwise component of wavenumber.

A third approach is based on the hypothesis of Corrsin (1951) that in the inertial subrange the one dimensional temperature spectrum can be expressed as

$$S_T(K) = \alpha x \varepsilon^{-1/3} K^{-5/3} \qquad (7)$$

where x is the rate of molecular destruction of $\langle (T-\bar{T}) \rangle_{av/2}$ (in $^{o}C^{2}S^{-1}$), ε is the rate of molecular dissipation of turbulent kinetic energy (in $cm^2\ s^{-3}$), and α is hypothesized to be a universal, dimensionless constant; the same in all flows. Equations (6) and (7) yield an expression for C_T^2 in terms of the rates of dissipation of turbulent kinetic energy and temperature variance, viz.

$$C_T^2 = \beta x \varepsilon^{-1/3} \qquad (8)$$

where β is an empirical constant with a value of 3.20.

C. MICROSCALE ℓ_o (OR ε)

Both ε and x in Equation (8) represent molecular processes and forces which act only over very small distances. As previously indicated, the particular scale length of interest in propagation analyses is the microscale of turbulence defined by Equation (6) and is dependent on only one dynamic parameter, the dissipation rate of turbulent kinetic energy, ε, which can be estimated from the one dimensional spectral density of velocity as

$$S_u(K) = \xi\ \varepsilon^{-2/3} K^{-5/3} \qquad (9)$$

where ξ is an empirical constant determined to be 0.51.

D. TAYLOR'S HYPOTHESIS

Because measurements are normally made at a point a relation between temporal (f) and wavenumber or spatial frequency (k) is required. According to Lin (1953), if one considers that eddies of wavenumber K are correlated only over distances not large compared to $2\pi/k$, then over such distances the non-uniformity of convection velocity should be small relative to the convection velocities. Further, if the mean velocity is a good approximation to the convection velocity, then $\bar{U} >> \bar{U}'$ where $\bar{U}'$ is the spatial gradient of $\bar{U}$. If these criteria are met the turbulence field may be considered as being frozen and swept at the mean wind speed $\bar{U}$ past a stationary instrument. This is known as Taylor's hypothesis and it allows frequency spectra to be interpreted as streamwise wavenumber spectra. This enables the evaluation of C_T^2 from Equation (6) using point temperature fluctuation measurements.

E. RELATING C_T^2 AND ε TO STABILITY PARAMETERS

Turbulence similarity theory relates both ε and x to measurable stability parameters so that C_T^2 can be estimated using Equation (8). The 1968 Air Force Cambridge Research Laboratory (AFCRL) boundary layer study yielded information on the behavior of both ε and x and the combination of dimensional and physical arguments that make up surface-layer similarity theory. The AFCRL results demonstrated that the statistics of both the mean and turbulent fields, when properly non-dimensionalized, are universal functions of the stability parameter (Z/L).

Non-dimensionalized ε and x values can be expressed as

$$\frac{z\varepsilon}{U_*^3} = f_1 (Z/L) \tag{10}$$

$$\frac{xz}{T_*^2 U_*} = f_2 (Z/L) \tag{11}$$

where the scaling velocity is $U_* = (-\overline{u'w'})^{\frac{1}{2}}$, the scaling temperature is $T_* = \frac{-\overline{w'T'}}{U_*}$, the Monin Obukhov stability length is $L = - T_o U_*^3 / kg\, \overline{w'T'}$ and $f_1(Z/L)$ and $f_2(Z/L)$ are empirically determined functions.

An empirical expression relating C_T^2 to boundary fluxes arises from direct substitution of Equations (10) and (11) into Equation (8) as

$$C_T^2 = T_*^2 \, z^{-2/3} \, f_3 (Z/L) \tag{12}$$

where $f_3(Z/L)$ is a combination of $f_1(Z/L)$ and $f_2(Z/L)$. The formulation of $f_3(Z/L)$ was examined by Wyngaard, et al. (1971) and their results are shown in Figure 1. They obtained the following forms for $f_3(Z/L)$

$$f_3(Z/L) = 4.9[1-7(Z/L)]^{-2/3} \quad 0 \geq Z/L \tag{13}$$

$$f_3(Z/L) = 4.9[1+2.75(Z/L)] \quad 0 < Z/L \tag{14}$$

where negative and positive Z/L values correspond to unstable and stable conditions respectively.

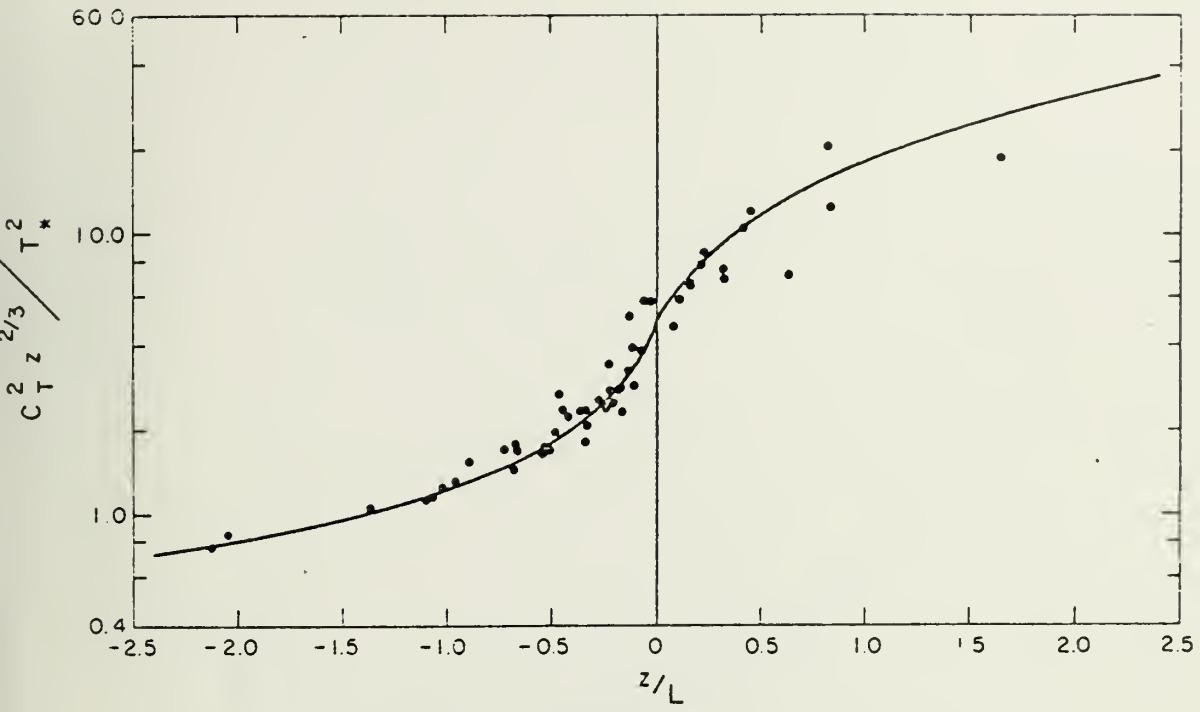

Fig. 1. The vertical profile of C_T^2.

An empirical expression relating ε to boundary fluxes is Equation (10), where $\phi_M(\frac{Z}{L}) - \frac{Z}{L}$ can replace $f_1(Z/L)$, viz.

$$\frac{\varepsilon Z K}{U_*^3} = \phi_M(Z/L) - Z/L \qquad (15)$$

where $\phi_M(Z/L)$ is the non-dimensional wind shear. Overwater results by Garrett (1972) on the non-dimensional dissipation rate, $K\varepsilon Z U_*^{-3}$, versus Z/L appear in Figure 2.

Both Equations (12) and (15) can be rewritten so that gradient terms appear in the non-dimensional C_T^2 and ε terms if the following expressions for T_* and U_* are used

$$T_* = \frac{KZ}{\phi_h(Z/L)} \frac{\partial \theta}{\partial z} \qquad (16)$$

$$U_* = \frac{KZ}{\phi_M(Z/L)} \frac{\partial u}{\partial z} \qquad (17)$$

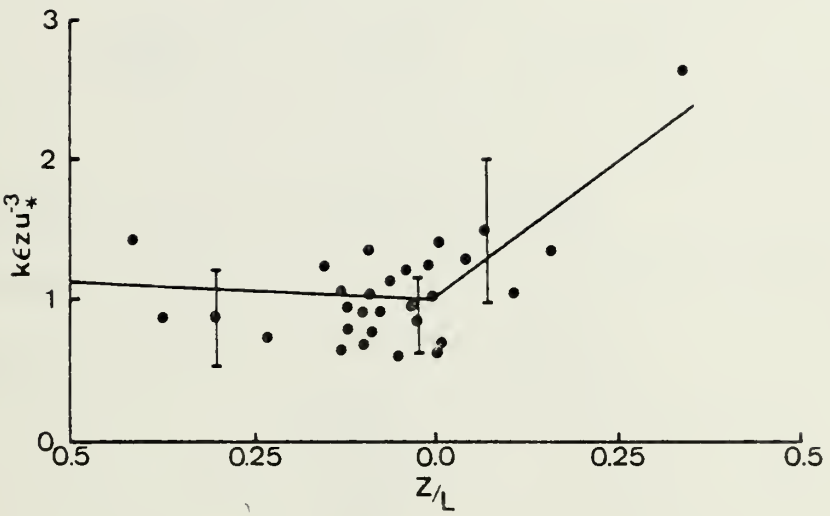

Fig. 2. The dimensionless dissipation rate versus Z/L.

Substituting Equation (16) into Equation (12) and Equation (17) into Equation (15) yield such expressions for the non-dimensional C_T^2 and ε terms respectively

$$\frac{C_T^2}{Z^{4/3}(\frac{\partial\theta}{\partial z})^2} = \frac{K^2}{\phi_h^2(\frac{Z}{L})} f_3(Z/L) \qquad (18)$$

$$\frac{\varepsilon}{Z^2(\frac{\partial u}{\partial z})^3} = K^2[\phi_M(\frac{Z}{L})^{-2} - \frac{Z}{L}\phi_M(\frac{Z}{L})^{-3}] \qquad (19)$$

F. RELATING Z/L TO RICHARDSON NUMBER

The above expressions can be interpreted more readily by relating Z/L to the Richardson number,

$$Ri = \frac{q(\frac{\partial\theta}{\partial z})}{T(\frac{\partial\bar{u}}{\partial z})^2},$$

as

$$Z/L = f_4(Ri) \qquad (20)$$

where $f_5(Ri)$ is an empirical function which has been well documented for the constant flux layer overland (Businger et al., 1971) and θ_v is the vertical potential temperature, $\theta_v = \theta(1 + .61\bar{q})$.

The following relationships between Z/L and Ri were determined by Dyer and Hicks (1970) for the unstable case and by Webb (1970) for the stable case:

$$\begin{aligned} Z/L &= Ri && Z/L < 0 \\ Z/L &= \frac{Ri}{1-\alpha Ri} && Z/L > 0 \end{aligned} \qquad (21)$$

Here α is an empirically derived constant equal to 5. These relationships have been recently verified for the overwater regime by Paulson, et al. (1972).

Combining Equation (18) and Equation (20) yields an expression for C_T^2 in terms of gradient measurements,

$$\frac{C_T^2}{z^{4/3}\left(\frac{\partial\theta}{\partial z}\right)^2} = f_6(Ri) \qquad (22)$$

The function $f_6(Ri)$ which has been determined for the overland constant flux layer is shown in Figure 3 (Wyngaard, et al., 1971).

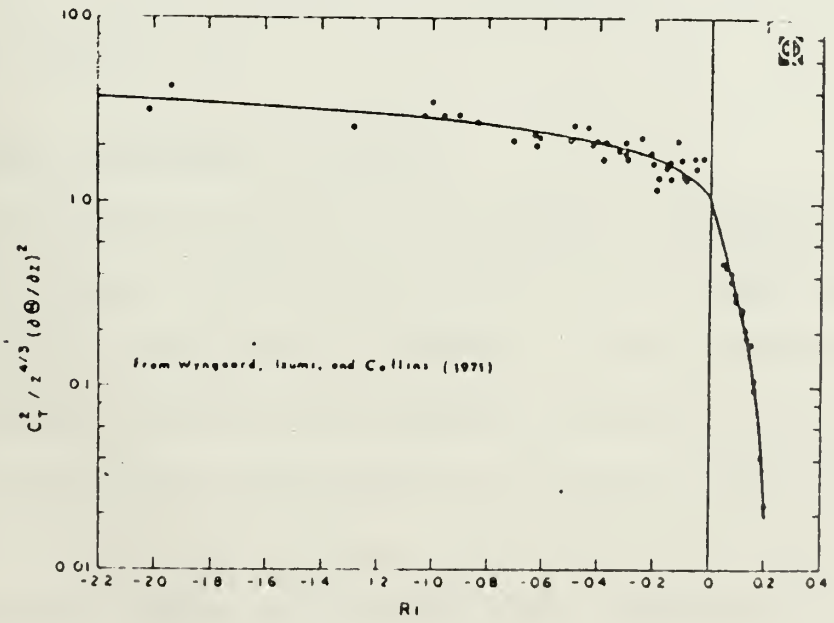

Fig. 3. The dimensionless temperature-structure parameter parameter versus the Richardson number.

Similarly, combining Equation (21) and Equation (19) yields the following gradient relationships for ε

$$\frac{\varepsilon}{Z^2(\frac{\partial u}{\partial z})^3} = K^2[(1-15Ri)^{\frac{1}{2}} - Ri(1-15Ri)^{3/4}] \quad Ri < 0 \qquad (23)$$

$$\frac{\varepsilon}{Z^2(\frac{\partial u}{\partial z})^3} = K^2[\{1+4.7\ (\frac{Ri}{1-5Ri})\}^{-2} - (\frac{Ri}{1-5Ri})\{1+4.7(\frac{Ri}{1-5Ri})\}^{-3}]$$

$$Ri > 0 \qquad (24)$$

The curve defined by these relationships will be presented later (Figure 22).

G. BULK AERODYNAMIC FORMULA

An alternate approach for indirect estimates of the turbulent fluxes in overwater observational experiments is the use of bulk aerodynamic formulae. A bulk aerodynamic formula is one which relates the boundary fluxes to the wind speed at a level and the temperature and humidity differences between that level and the surface. Such formulae require several assumptions regarding the stability conditions of the boundary layer and the turbulent processes within it.

Bulk aerodynamic formulae for momentum (U_*^2), sensible heat ($\overline{wT'}$) and humidity ($\overline{wq'}$) fluxes have the following forms,

$$U_*^2 = C_D \bar{U}^2 \tag{25}$$

$$w'\theta = C_H \bar{U}(T_a - T_s) = C_H \bar{U}\Delta T \tag{26}$$

$$\overline{w'q'} = C_E \bar{U}(Q_a - Q_s) = C_E \bar{U}\Delta Q \tag{27}$$

where the symbols have been defined on page 11.

Friehe (1976) summarized considerable amounts of recent overwater data to obtain overwater estimates of C_D, C_H, and C_E. He observed C_H and C_E to be dependent on the values of $\bar{U}\Delta T$ as well as height z. Friehe used the bulk aerodynamic formulae to formulate an alternate expression for the estimation of Z/L in the atmospheric boundary layer above the sea. The formulation consisted of replacing the transfer terms (T_* and U_*) in the expression for L by bulk parameters ($U_*^2 = C_D U_{10}^2$ and T_*) to obtain

$$\frac{Z}{L} = -.231\left[\frac{z\Delta T}{\bar{U}^2} + 0.212\,\frac{z\Delta Q}{\bar{U}^2}\right] \qquad -20 < \bar{U}\Delta T < 25 (mKs^{-1})$$

$$\frac{Z}{L} = -.371\left[\frac{z\Delta T}{\bar{U}^2} + 0.132\,\frac{z\Delta Q}{\bar{U}^2}\right] \qquad \bar{U}\Delta T > 25 (mKs^{-1}) \tag{28}$$

Equation (28) leads to a new stability parameter X, defined as

$$X = \frac{z\Delta T}{\bar{U}^2}\left(1 + 0.212\,\frac{\Delta Q}{\Delta T}\right) \qquad -20 < \bar{U}\Delta T < 25 (mKs^{-1})$$

$$X' = \frac{z\Delta T}{\bar{U}^2}\left(1 + 0.132\,\frac{\Delta Q}{\Delta T}\right) \qquad \bar{U}\Delta T > 25 (mKs^{-1}) \tag{29}$$

Note that the signs of X and X' are the same as Z/L.

Friehe defined X and X' for the 10 meter level. However, these can be generalized to any level by the approximation

$$\frac{C_D(z)}{C_D(10)} = \frac{C_H(z)}{C_H(10)} = \frac{C_E(z)}{C_E(10)} = \left[\frac{L_N(\frac{10}{Z_o})}{L_N(\frac{z}{Z_o})}\right]^2 \qquad (30)$$

This was done in this study.

Substituting Equations (28) and (29) into Equation (12) yields for $-20 < \bar{U}\Delta T < 25 (mKs^{-1})$

$$\frac{C_T^2 Z^{2/3}}{(\Delta T)^2} = \begin{cases} 3.12 \times 10^{-3}(1+1.62X)^{-2/3} & \text{unstable} \\ 3.12 \times 10^{-3}(1-0.635X) & \text{stable} \end{cases}$$

for $\bar{U}\Delta T > 25 (mKs^{-1})$

$$\frac{C_T^2 Z^{2/3}}{(\Delta T)^2} = 8.03 \times 10^{-3}(1+2.60X')^{-2/3} \qquad (31)$$

III. EXPERIMENT

A. PLATFORM AND LOCATION

Observations aboard the R/V Acania during the experiment in September and October 1976 were made in the area from 32° 15'N to 34°13'N and 123°18'W to 120°20'W; Figure 4. This area provided a good sample for open ocean condition.

B. INSTRUMENTATION

Ten minute averages of temperature, wind, and relative humidity were taken at four levels, on two separate masts spatially separated on the forward deck of the ship, Figure 5.

1. Recording

Data logging during the experiments was accomplished using the NPS developed MIDAS (Microprogrammable Integrated Data Acquisition System). This micro-processor based data acquisition system utilizes an Intel 8008 central processor to control the sampling, averaging, and recording of mean meteorological data. All software is written in PL/M to facilitate the writing of self-documenting program.

2. Mean Measurement Systems

Mean wind measurements were made with a Thornthwaite Associates cup anemometer wind profile register system, model number 104, Figure 6. In operation, the shaft of a three cup anemometer unit serves as the shutter between a light source and a photocell for each revolution. These three plastic

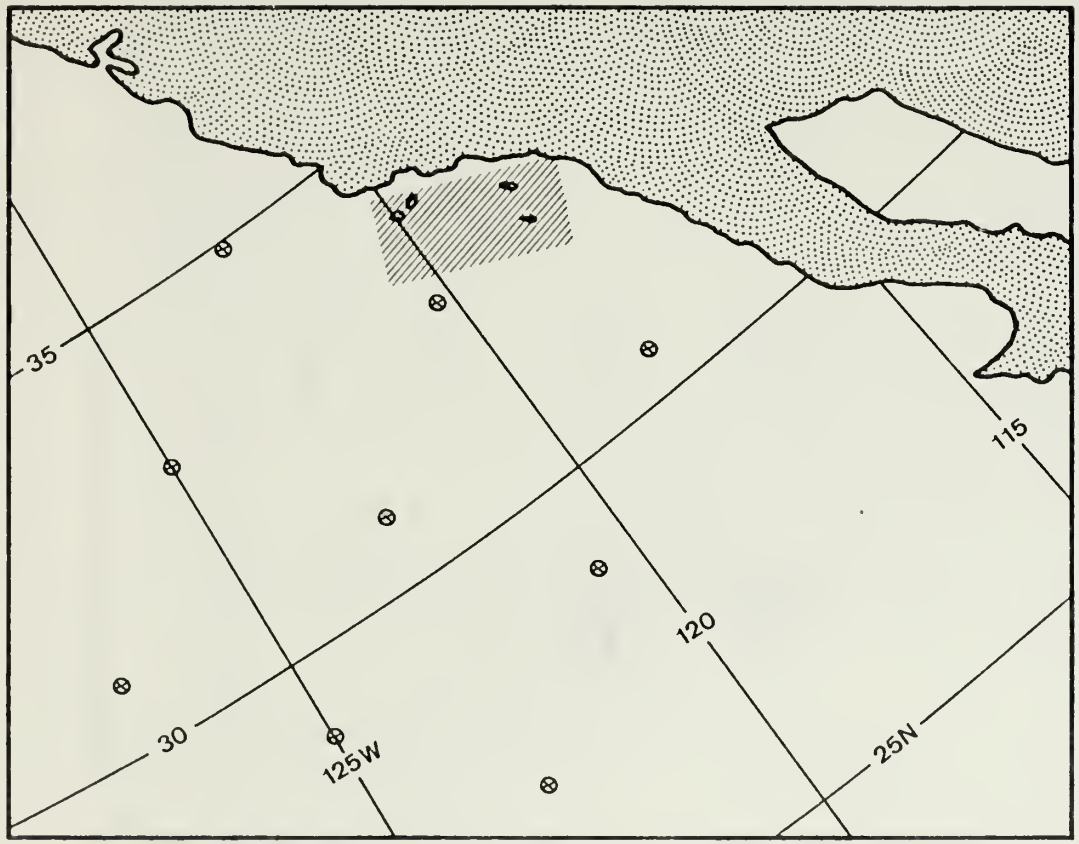

Fig. 4. Experimental area of R/V Acania.

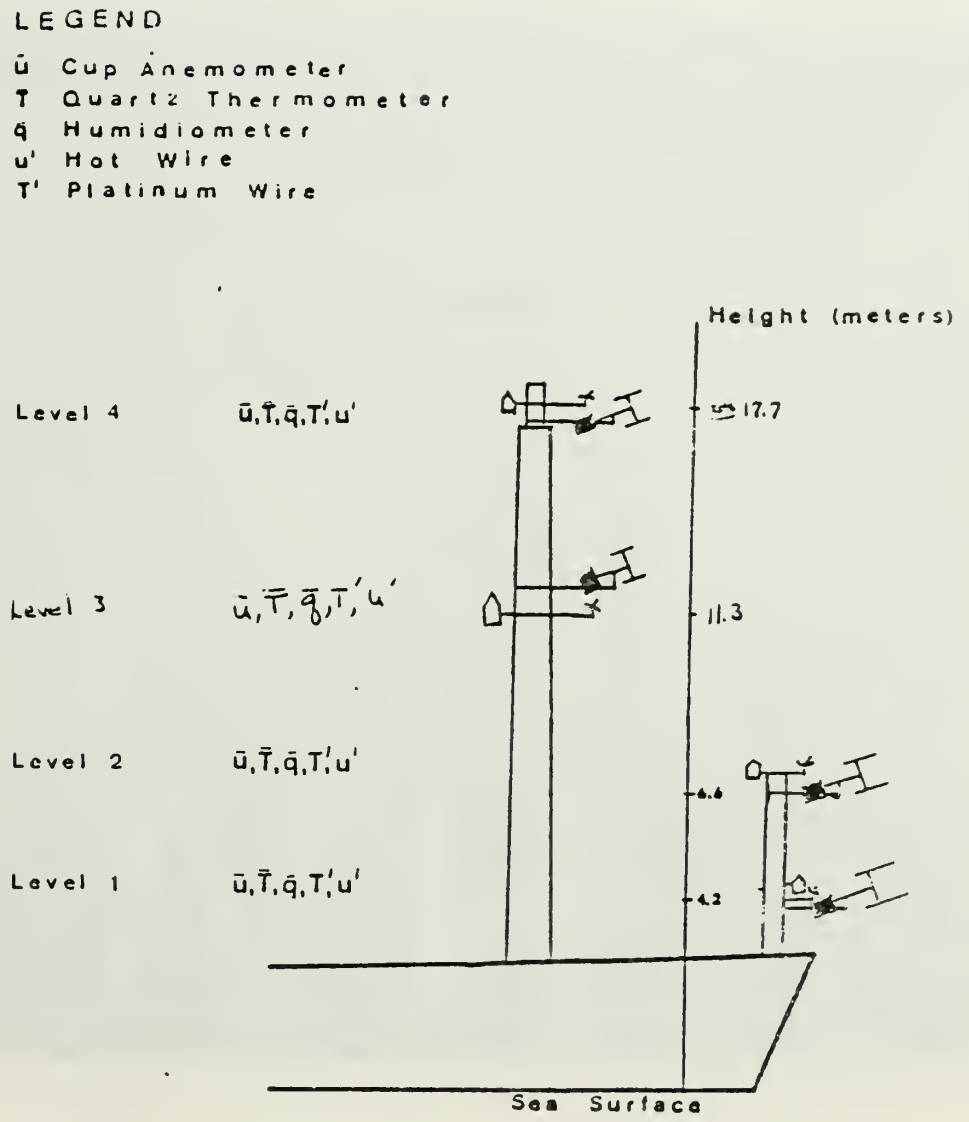

Fig. 5. Mounting arrangements aboard the Acania.

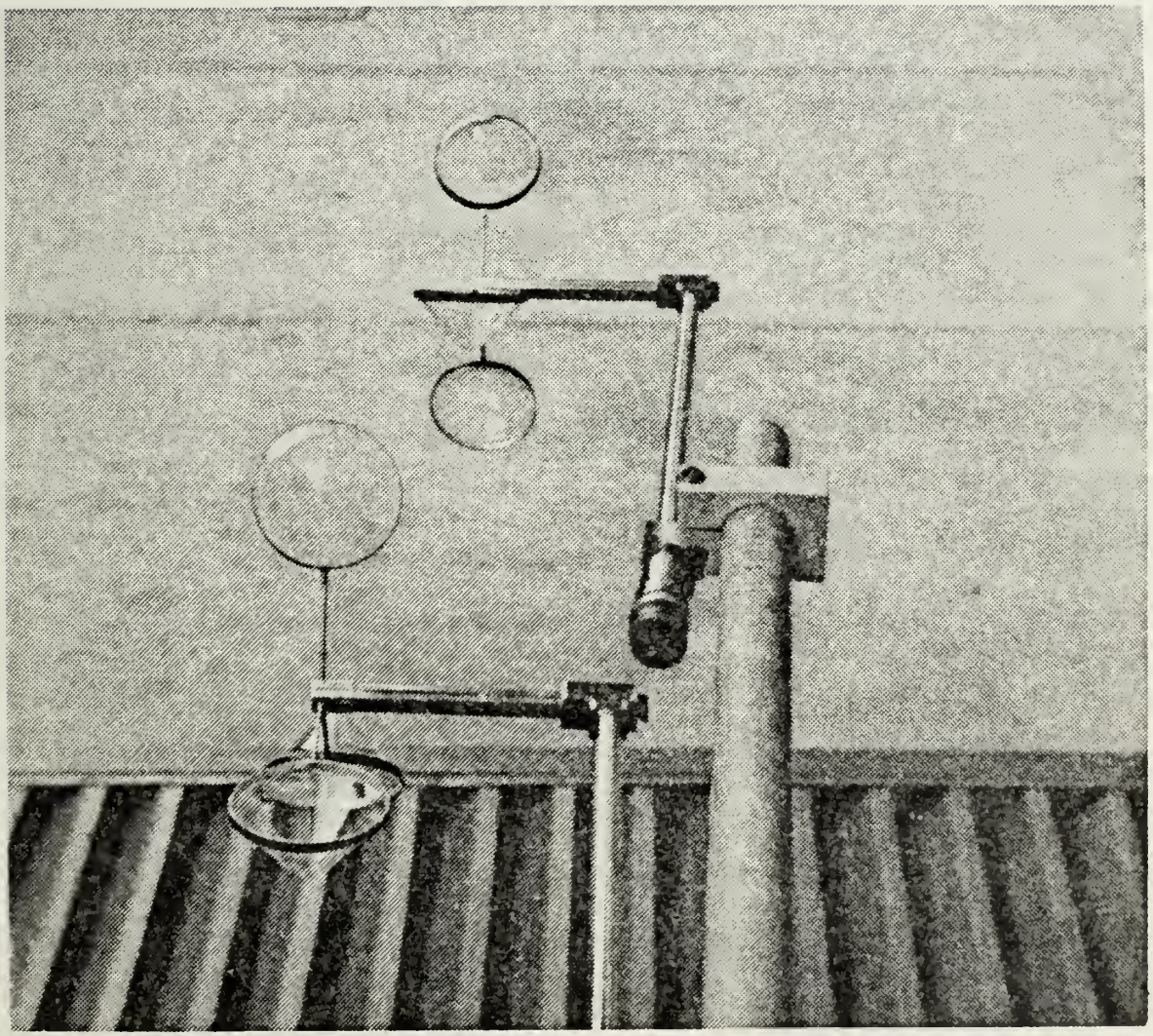

Fig. 6. Thornthwaite Associates Cup anemometer wind profile register system.

cone cups are reinforced with aluminum frames and are mounted at 120° intervals on stainless steel tubes attached to the main shaft. A characteristic of these cup anemometers is low starting speeds with a small amount of internal friction which aids in checking inertial overshoot.

Mean temperature measurements were made with temperature sensitive quartz crystal probes, (Hewlett Packard model HP-2850) at each level. (Figure 7) RF signals from the crystal probes and from a reference oscillator were mixed in the HP-2801A readout unit to produce a beat frequency whose signature can be analyzed to within 0.001 degrees centigrade per hertz. Each sensor simultaneously received pre-experiment calibration against a platinum resistance wire thermometer in a temperature controlled circulating water bath over the expected temperature range. The accuracy in achieving a 0.005 degree centigrade correction factor was a constant for each probe. A 3.7 meter flexible coaxial cable is permanently attached to the sensor head and the mast mounted probes are housed in an aspirated shelter as seen in Figure 8. Temperature values were automatically recorded on a printed tape.

Mean relative humidity was obtained using the Dunmore-lithium chloride sensor and Hygrodynamics Digital I hygrometer indicator. (Figure 9) The sensor was also placed in the aspirated shelter. The basis of operations of this system is resistance charge within an electrolytic solution generating a reference voltage variance proportional to the relative humidity change. Automatic temperature compensation in the instruments meet the following specifications

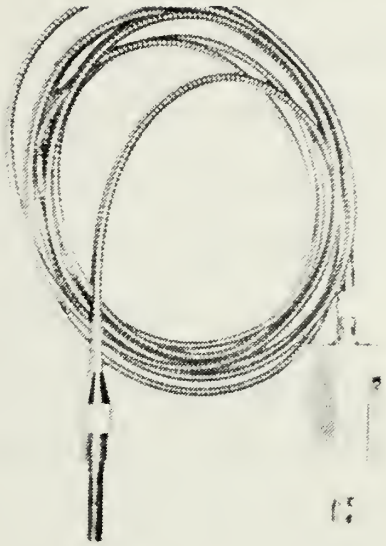

Fig. 7. Hewlett Packard model HP-2850 temperature sensitive quartz crystal probes.

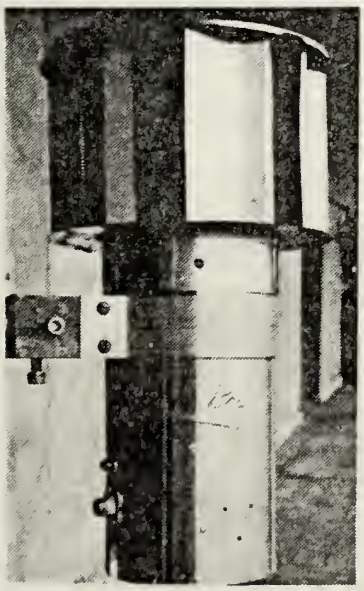

Fig. 8. Aspirated shelter.

Fig. 9. Dunmore type lithium chloride humidity sensor.

± 3% relative humidity below 90%

± 4% relative humidity below 90%

Calibration of sensors was accomplished by a comparative method using a saturated saline solution in a closed container. Observation and recording was accomplished in like manner as the temperature.

3. Fluctuation Measurements

The temperature fluctuations were measured using a bridge developed at GTE Sylvania, the GTE Sylvania Model 140. It was necessary to modify the system slightly for use aboard the R/V Acania.

This system is a small temperature difference sensing device originally designed to be carried aloft by a balloon and equipped to process and transmit, by pulse-rate modulation on a radio frequency carrier, this information to a ground-base receiving station for demodulation and recording.

The baseband portion of this system is a balanced Wheatstone bridge excited by a 3KHZ signal with a synchronous detector on the output. Segments of a very small diameter platinum wire serve as temperature sensors in opposite arms of the bridge. In the single wire mode, one wire is replaced by fixed resistance. An output from the bridge which is proportional to the temperature difference between the two probes or a temperature change of a single wire in the single wire mode is produced.

The sensor wire is 0.5 cm long and 2.5×10^{-6}m in diameter. This extremely small mass allows a response to

temperature variations of up to 1 KHZ while electronic amplification allows temperature difference as small as 0.004 degrees C to be observed.

Wind fluctuations were recorded on a Honeywell model 5200 14 channel tape recorder. Real time readout on an eight channel chart recorder, Brush model 240, was used to check the quality of the signals coming from the sensors.

4. Fluctuation Statistics

Spectral analyses to obtain values were performed on fluctuating velocity data obtained with Hot Film sensors oriented in the vertical, normal to the mean wind. These data represent a point measurement and yield temporal or time descriptions of the fluctuations. Ten minute segments of data originally recorded on magnetic tape were recorded into an EMR-Schlumber model 1510 digital spectrum analyzer. Procedures for converting spectral values, obtained with the analog spectral analyzer, to engineering units and for obtaining turbulence parameters from the spectra are described in the following paragraphs:

a. Scaling Spectral Plots

A necessary procedure was scaling the spectral plots to relate RMS input voltages to power spectral densities (PSD); variance per unit frequency. To obtain power spectral density levels, corresponding to RMS voltage inputs, calibrated scale charts had to be constructed.

For purposes of the x-y plot format of the analyzer output, the RMS voltages were converted to $y = \log_{10}$

(voltage) units and a graduated scale was constructed so that the logarithm of volts RMS could be interpolated from spectral plots. The value of the vertical scale (y) was adjusted for each spectrum as a function of both input gain and spectral gain. These values were then converted to PSD levels for use in calculating ε values.

The relation between Volts RMS to PSD units used was

$$S(f)\ \text{PSD units} = \frac{(\text{cal. level VRMS})^2}{1.5\ \text{Bandwidth}} \times (10^y)^2 \qquad (32)$$

where $\text{Bandwidth} = \frac{\text{Freq. Range}}{\text{No. Channels}}$

$$\left(= \frac{256\ \text{Hz}}{\text{Hz}} = 1\ \text{Hz} \right)$$

and cal. level VRMS = voltage at y = 0

(= 1 VRMS for 3.16 V input setting).

Amplitude scaling calibrations were accomplished using externally generated "white noise" signals of 1 Volt RMS with a frequency range from 0.1 Hz to 1000 Hz (giving a PSD of $10^{-3}V^2/Hz$). Setting a 3.16 V (10dB) input on the EMR 1510 Digital Spectrum analyzer insures that 1 Volt corresponds to y = 0. An example of such a calibration plot for a frequency range of 1-200 Hz (the frequency range of interest) is shown in Figure 10.

b. Computation of Turbulence Parameters from Scaled Spectra

Values of the turbulence parameter ε were obtained from the velocity variance spectra on the basis of the formula

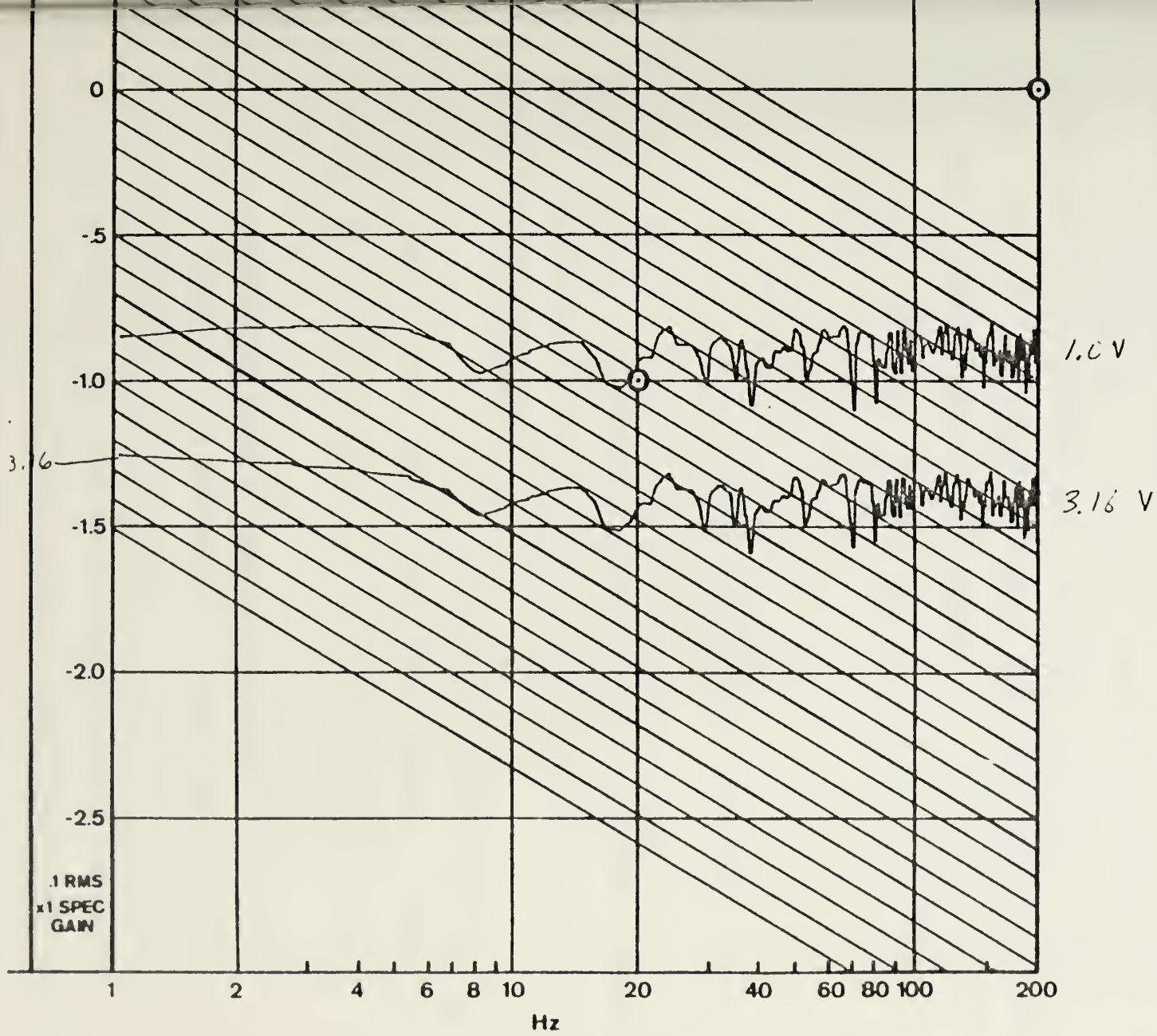

Fig. 10. Spectrum calibration plot.

for the inertial subrange in wave number space S(k), Equation (6), which predicts a -5/3 slope for the spectra when plotted in a log-log format. Figure 11 is a typical spectra considered in the analyses. Velocity variance spectra consistently exhibited slopes of -5/3.

Assuming -5/3 slopes for the variance spectra, the intercept of the best fit -5/3 slope with the 1 Hz frequency line was the spectral density denoted (PSD) value used in computing the parameter of interest, ε. The measured PSD value was converted to engineering spectral density units by the relation

$$S_u(f) = C_u^2 \cdot PSD$$
$$= (cm/s/Volt)^2 \cdot Volt^2/Hz = (cm/s)^2/Hz \quad (33)$$

where C_u was the calibration factor for the constant temperature, anemometer. Determination of the value for C_u has been described by Lund (1975).

Since the velocity fluctuations were measured at a fixed point in the flow, the resultant spectral values are defined at "temporal" frequencies denoted as $S_u(f)$ in Equation (33).

5. Analysis of Paired Temperature Sensor

C_T^2 values were estimated by using paired platinum wire sensors for variance analysis. This analysis was based on the expression for the temperature structure function, Equation (5). The analysis is one in which temperature differences between the paired resistance wires separated by a

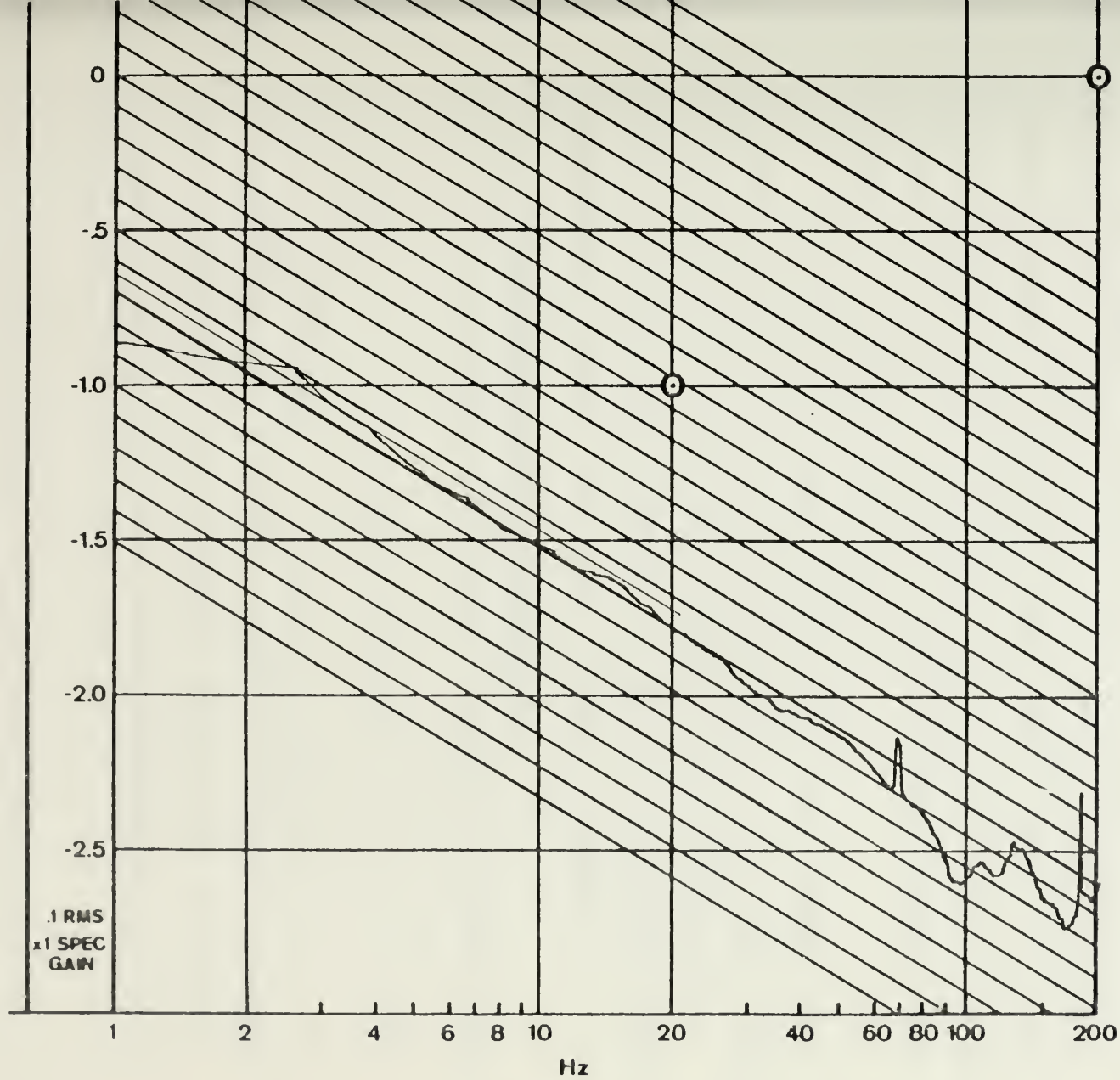

Fig. 11. Velocity spectrum.

distance r is subjected to variance analyses as indicated by the term $(T'(x) - T'(x+r))^2$.

Voltages corresponding to the temperature differences, ΔT, as measured by the paired sensors were recorded on analog magnetic tape. The variance or root mean square of the temperature differences required to compute C_T^2 was obtained by analyzing the analog voltages with a mean square voltmeter (Thermo Systems Incorporated, model 1060) using a 30 second time constant for the averaging. The output of the mean-square voltmeter (as well as a record of the original signal) were recorded on standard strip charts.

Ten minute averaged values of the RMS voltages were abstracted from the strip chart and these values were utilized in a program for the IBM 360 computer. This program converted the mean square voltages values to temperature difference variance values, from which C_T^2 were computed.

6. Fluctuating Sensor Calibration

Platinum wire resistance is related to temperature by

$$R = R_o(1 + \alpha(T-T_o)) \qquad (34)$$

where R = resistance, T = calibration temperature, $T_o = 0^oC$, R_o = resistance at T_o, and $\alpha = .0036/^oC$ (temperature coefficient of resistance for platinum). Each wire's resistance was measured in the laboratory at a temperature T, to determine R_o.

Temperature fluctuations can be related to wire resistance fluctuations by differentiating Equation (34)

$$dR = \alpha R_o dT$$

or

$$R' = \alpha R_o T' \tag{35}$$

Recorded voltage fluctuations are then related to resistance changes by the transfer function, H, in the expression

$$V' = HR' \tag{36}$$

where H was determined for the bridges by varying the resistance of a TSI 1056 Variable Decade Probe Resistance and recording the corresponding voltage changes. Voltage vs resistance is plotted and the slope of this plot determines the transfer function, H. For this experiment H = 10 volts/ohms.

Finally, to relate recorded voltage fluctuations to temperature fluctuations, Equation (36) is substituted into Equation (35) giving

$$T' = (1/H\ R_o)\ V' \tag{37}$$

or

$$T' = C_H V' \tag{38}$$

where C_H is the temperature calibration factor in ^{o}C/volt.

Velocity sensors calibrations were accomplished in a wind tunnel using the Hot Wire Calibrator TSI 1125. In this process, a known wind velocity is blown across the wire and the corresponding voltage output is recorded. The sensor wind speed is given by

$$V^2 = a\bar{U}^{1/2} + b \tag{39}$$

where V is the hot-film voltage output and $\bar{U}$ is the mean wind speed for any given level. The constants, a and b, are the calibration curve slope and intercept respectively. The constants, a and b, were derived in the lab.

To convert the voltage PSD levels to velocity units requires a calibration factor given by

$$U' = CV' \tag{40}$$

where C is the calibration factor in m/s/volt, V' is the voltage fluctuation, and U' the velocity fluctuation.

Differentiating Equation (39) yields

$$U' = (4V\bar{U}^{1/2}/a)\ V' \tag{41}$$

which when substituted into Equation (40) yields

$$C = 4V\bar{U}^{1/2}/a \tag{42}$$

The slope of the plotted curve yields the value for a in the above equation.

C. ANALYSIS PROCEDURES

The data were edited for gross errors or inconsistencies due to known instrumentation malfunctions or limitations of instruments. An example of limitation on instruments is the relative wind direction being greater than 30° off the bow of the ship. Earlier experiments have shown that when these conditions exist, the winds are greatly influenced by the ship and therefore are of little value to the experiment.

The criteria for evaluating or discarding data from individual levels or for entire interval depended on performance check results obtained during measurements, obvious inconsistencies, and the availability of fluctuation data. Since mean wind $\bar{U}$, mean temperature $\bar{T}$, and mean humidity $\bar{q}$, are expected to vary logarithmically with height, these parameters were plotted for each time period using the IBM 360 and NPS FORTRAN program PLOTP. A best fit straight line was drawn to the data points. (See Figure 12.) This procedure was very subjective, but was intended to further refine the data by detecting more obvious discrepancies and determining if the data did indeed vary logarithmically with height. Gradient values of the parameters used in actual computations were evaluated using a least square fit. By means of the subjective procedure, it was determined that the humidity sensor at the second level was reading too low during most of the experiment. (See Figure 11a.) This error was corrected for the least square fit by assigning the second level the same value as level three.

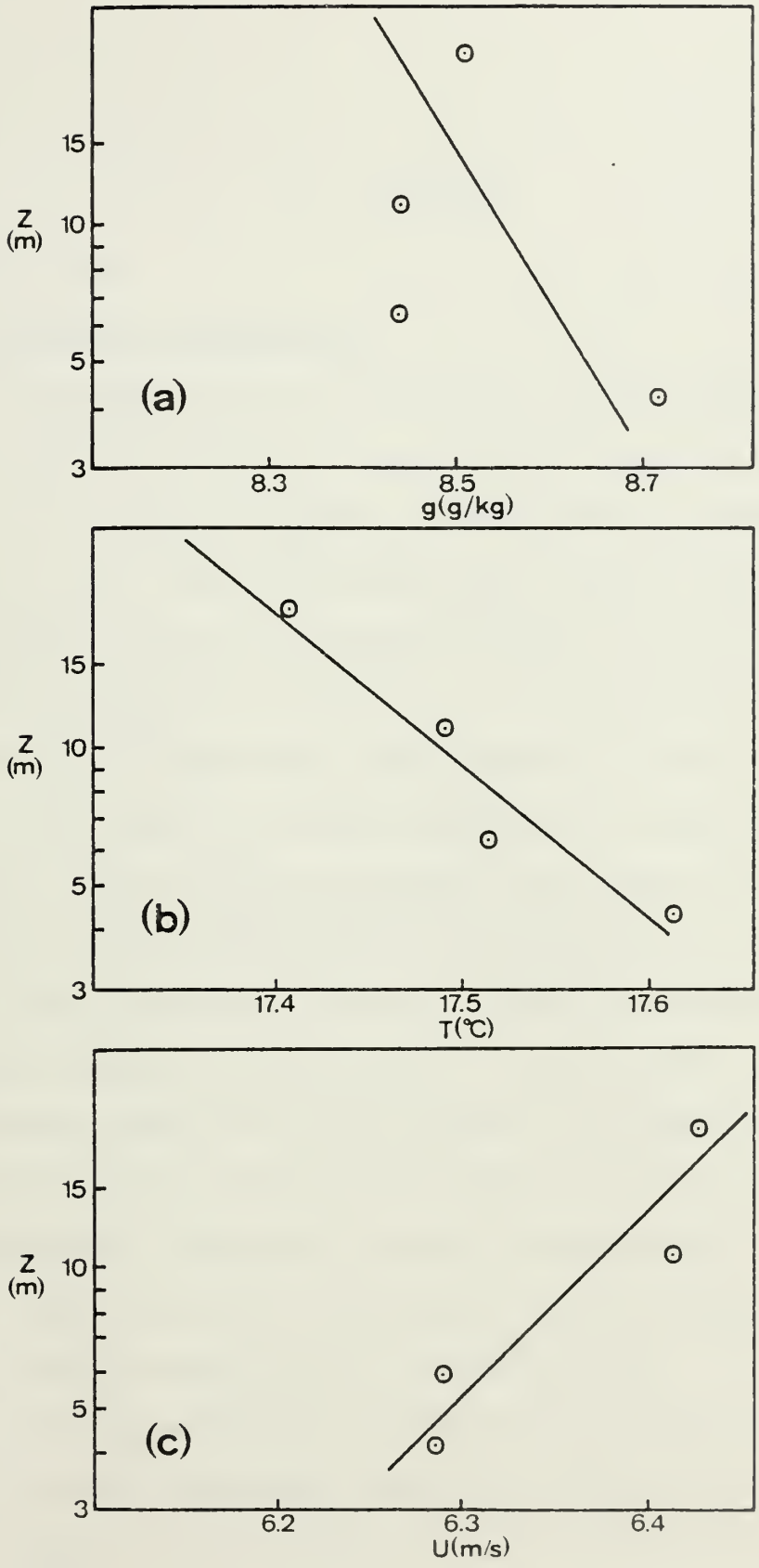

Fig. 12. Typical profiles for a) specific humidity - 25 Sept 75 (0105); b) temperature - 25 Sept 75 (0250); and c) winds - 25 Sept 75 (0551).

IV. RESULTS

A. C_T^2 RESULTS

1. Gradient Description

A comparison of 368 overwater C_T^2 and profile results with the overland empirical expression, Equation (22), appears in Figure 13. The distribution predicted by Equation (22) is the solid line. The circles are mean dimensionless temperature structure function parameter (DTSFP) results over .50 Richardson number (Ri) intervals. The Standard deviation corresponding to each mean value appears as vertical lines on which the number of values defining the mean appears. Significantly, these results represent more than a factor of 3 (368 versus 119) of those presented previously. (Davidson, et al., 1976). However, the mean DTSFP distribution changed very little between the two sets. Larger DTSFP values for the overwater regime for near neutral and stable conditions (Ri > -.5) can be qualitatively related to the wave influence. Decreased DTSFP values for unstable conditions (Ri < -.5) are, perhaps, associated with aerodynamic smooth properties for the sea surface during light wind conditions.

A curve describing the observed data was obtained using a best fit polynomial analysis. The results of this analysis were

$$= 2.37(.74+Ri)^{-5.04} \quad Ri \geq 0 \qquad (43)$$

$$C_T^2/Z^{4/3}(\frac{\partial\theta}{\partial z})^2 = 0.56(.24+Ri)^{-2.13} \quad -1.25 < Ri < 0 \qquad (44)$$

$$= 0.2 \quad Ri < -1.25 \qquad (45)$$

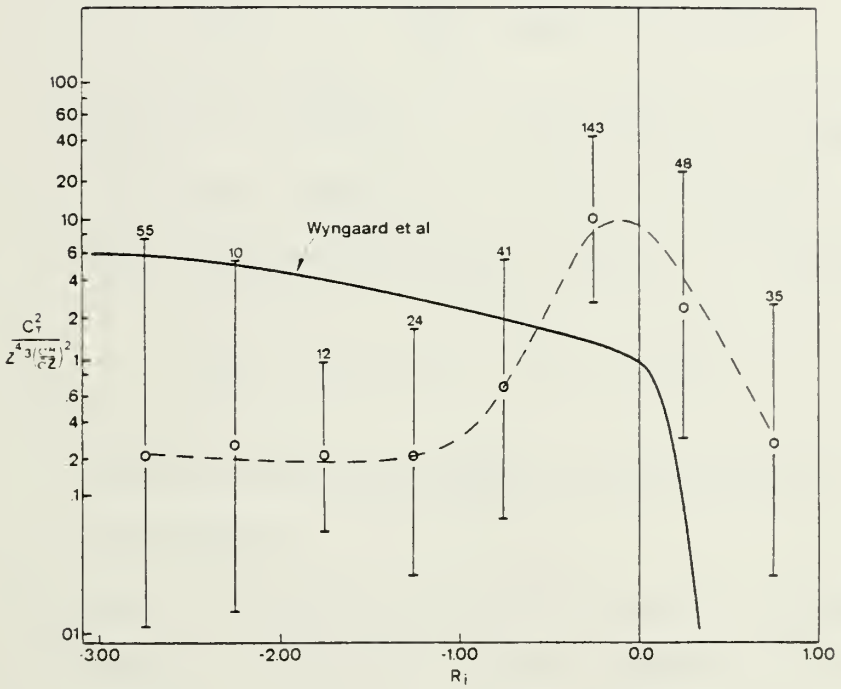

Fig. 13. Overwater results for DTSFP versus Richardson number.

The influence of the waves can be further examined on the basis of observed height variations of C_T^2. Similarity theory predicts that C_T^2 has a height variation which depends on stability which was discussed by Wyngaard et al. in conjunction with an examination of Equation (12). Since T_*^2 is independent of height in the surface layer, Equation (12) yields the following general predictions for the variation of C_T^2 with height based on stability.

a. For near neutral conditions, $(Z/L = 0)$, C_T^2 decreases with height as $Z^{-2/3}$ Equation (12) becomes

$$C_T^2 = T_*^2 \, Z^{-2/3} \qquad (46)$$

b. For unstable conditions ($Z/L \leq 0$, Equation (13)), C_T^2 decreases more rapidly with height than $Z^{-2/3}$. If $-7Z/L >> 1$, C_T^2 would decrease with height as $Z^{-4/3}$, since Equation (12) becomes

$$C_T^2 \approx 4/3 \frac{T^{2/3}}{kg} (\overline{wT'})^{4/3} Z^{-4/3} \qquad (47)$$

with $T^{2/3}/kg(\overline{wT'})^{4/3}$ independent of height.

c. For stable conditions ($Z/L \geq 0$), C_T^2 will decrease with height less rapidly than $Z^{-2/3}$ since

$$C_T^2 = T_* 4.9Z^{-2/3}[1+2.75 \frac{Z}{L}] \qquad (48)$$

and the term in brackets increases with increasing height.

The wave influence can also be seen in height versus C_T^2 or C_N^2 (computed from C_T^2 values) results in Figures 14 and 15 respectively. In Figure 14, the feature which suggests the wave influence is the departure from the $Z^{-2/3}$ height distribution as the surface is approached. In the upper three levels C_T^2 appears to fit a $Z^{-2/3}$ distribution, but as the surface is approached the distribution appears to be better defined by a $Z^{-4/3}$ height distribution. In Figure 15, a similar change is observed. The upper levels appear to fit a $Z^{-2/3}$ distribution for C_N^2 but as the surface is approached especially at the one meter level, the C_N^2 values appear to fit a $Z^{-4/3}$ height distribution.

Further evidence of wave influence on C_T^2 appears in joint probability-conditional mean results of the normalized

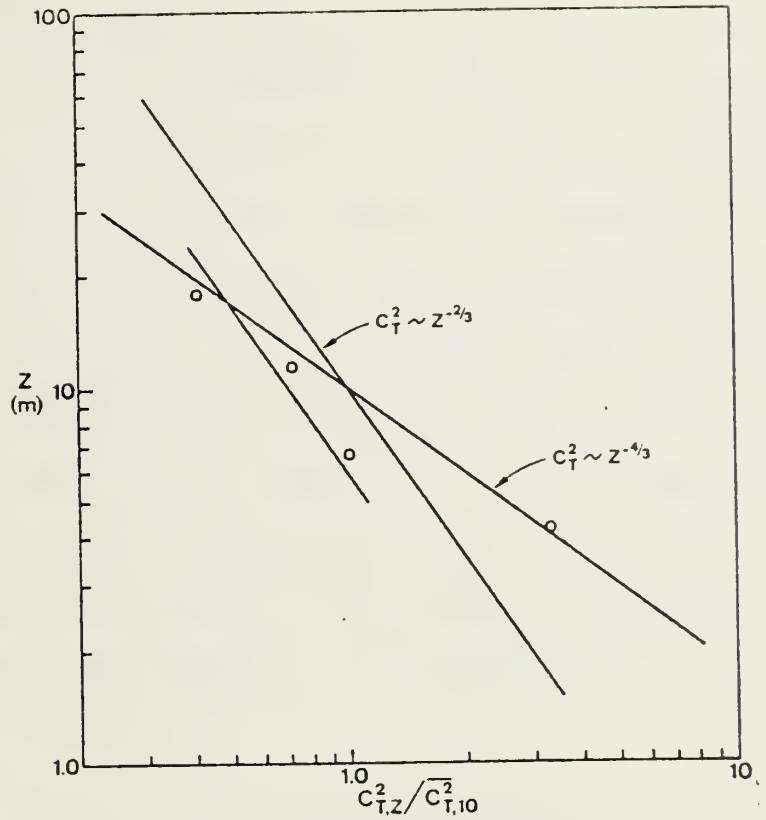

Fig. 14. Normalized C_T^2 results versus height (Z), 114 periods.

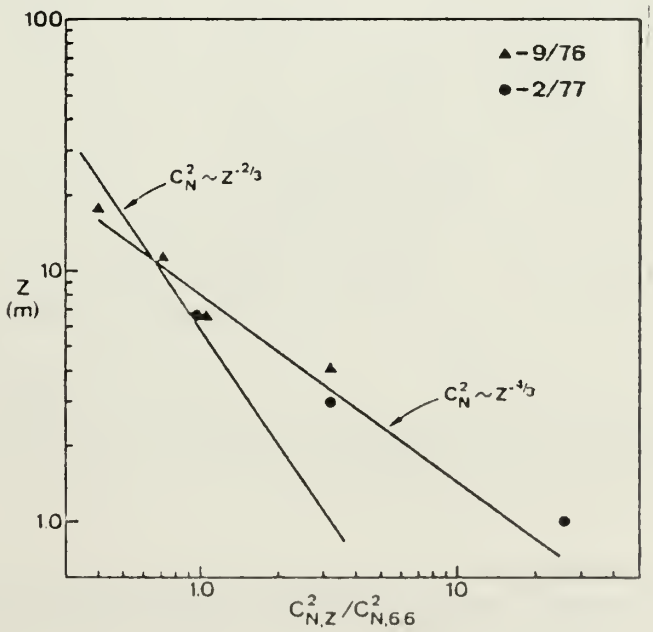

Fig. 15. Normalized C_N^2 (computed from C_T^2) results versus height.

temperature variance (σ_T/T_*) over waves in Figure 16. The results and the measurements yielding them have been described by Davidson (1974). The ratio $(\sigma_T^2/T_*)^2$ is directly related to the DTSFP, defined by Wyngaard, et al. (1971). In Figure 16, the vertical axis variable (C/U_*) defines wave influence on σ_T/T_*, C is the phase speed of prevailing swell, L is the Monin-Obukhov stability length. The results were obtained under stable conditions. The diagonal orientation of the contours of the number joint occurrences provides qualitative evidence that the waves' influence (C/U_*) on σ_T/T_*, hence the DTSFP, is as significant as the stability influence (Z/L).

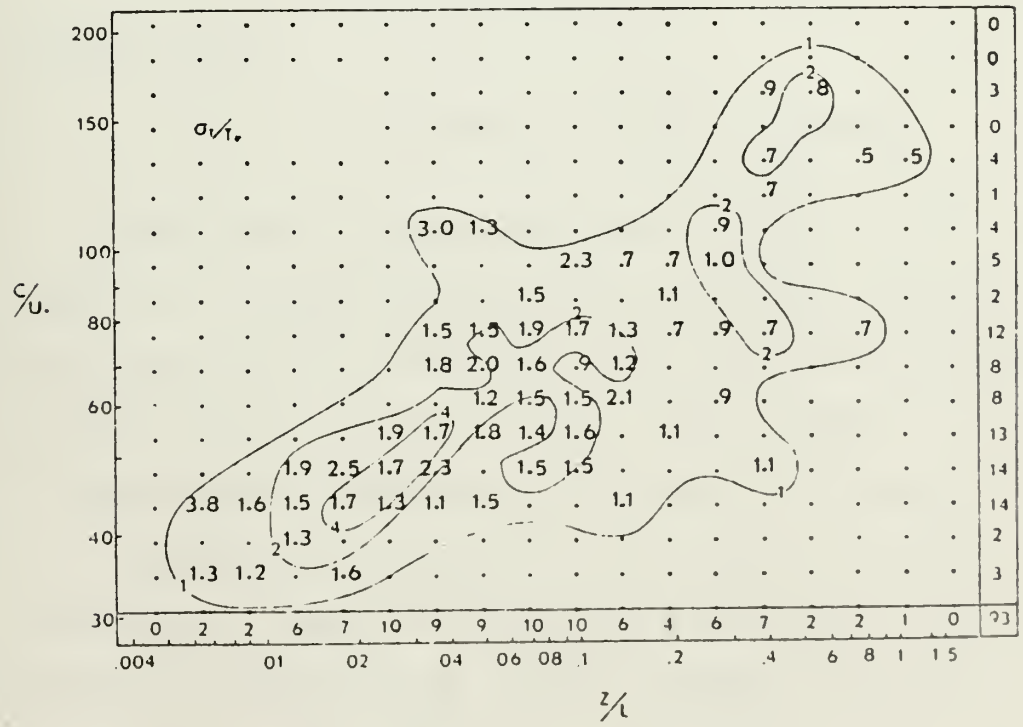

Fig. 16. Joint probability-conditional mean results of σ_T/T_* for C/U_* and Z/L dependence.

2. Bulk Aerodynamic

Results obtained from analyses with bulk aerodynamic variables, Equation (31), are compared to the Wyngaard et al. prediction curve in Figure 17. The latter is the solid line. The circles are mean dimensionless structure function parameter results over 1.00 X intervals. Standard deviations corresponding to mean values appear as vertical lines and the number above these vertical lines indicates the number of values defining each mean. Larger values of DTSFP are again attributed to the wave influence as explained earlier.

The following was evaluated for the bulk aerodynamic expressions using a best fit polynomial analysis.

$$C_T^2 Z^{2/3}/(\Delta T)^2 = .037(.642+X)^{-1.72} \quad \text{Stable} \qquad (49)$$

$$= .042(.323-X)^{-.57} \quad \text{Unstable} \qquad (50)$$

Three points from an analysis by Friehe (1976) appear in Figure 17. A significant aspect of Friehe's analysis of available data was the exclusion of C_T^2 data from temperature fluctuation records which contained large numbers of spikes exhibiting ramplike signatures, as shown in Figure 18. This led to a significant reduction in the amount of data used in his comparison. Based on observations by Hicks (1972) and hypothesis of Schmitt et al. (1976), Friehe attributed the occurrence of the spikes to salt nuclei accumulations on the wires with subsequential erroneously sensed temperature changes by the system as water vapor is absorbed or is evaporated on the salt nuclei.

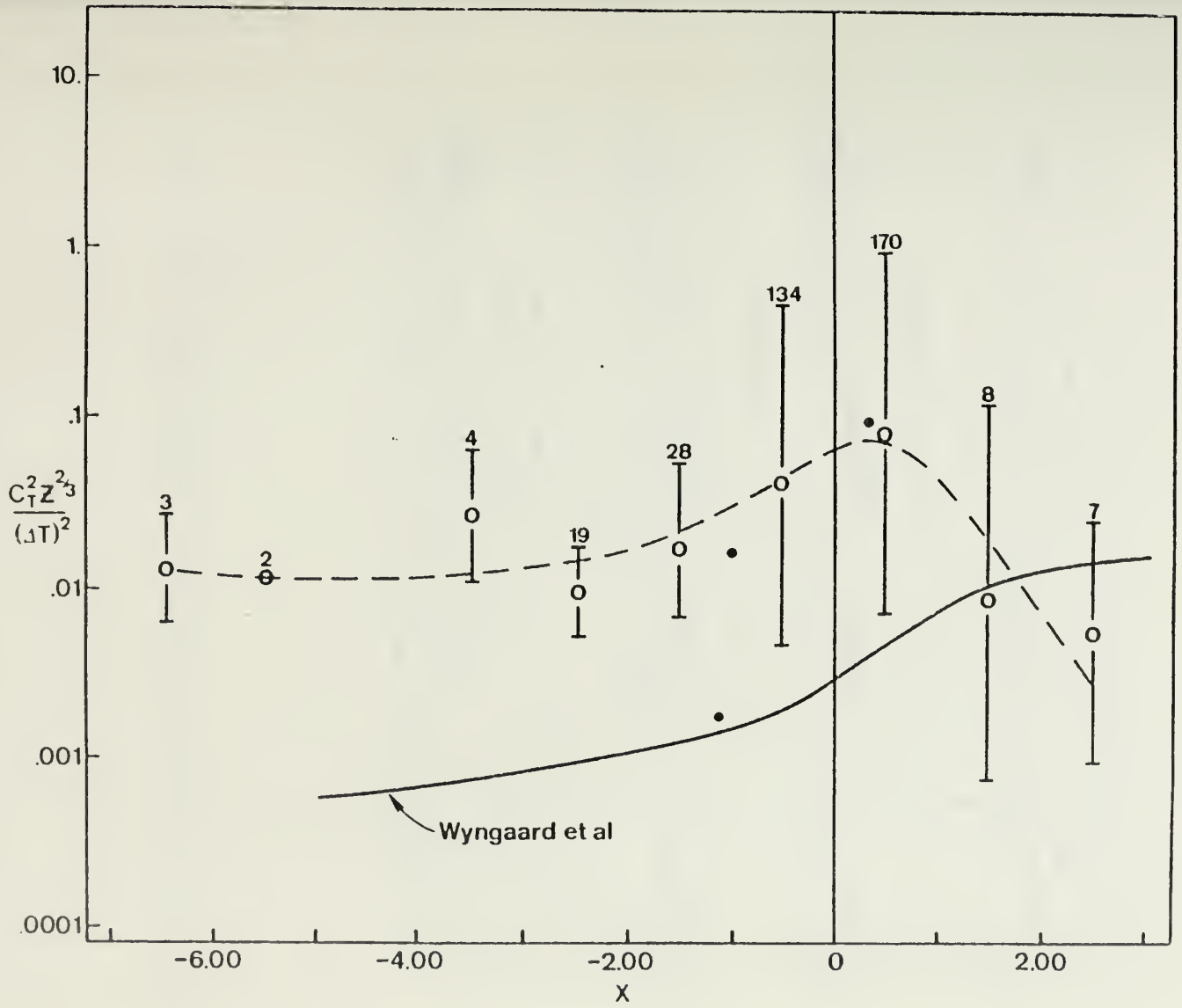

Fig. 17. Overwater results for dimensionless temperature-structure parameter versus X.

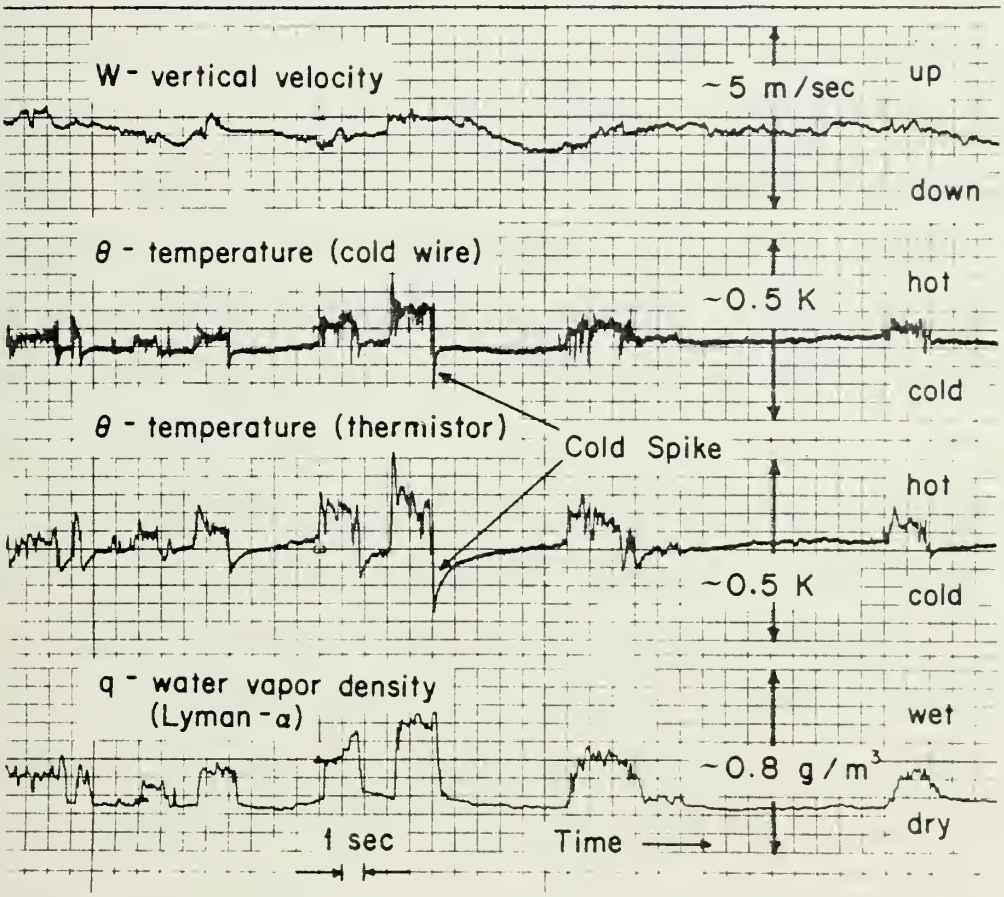

Fig. 18. Time series showing "cold spikes" in the temperature field under stable conditions.

The occurrence and nature of the spikes were also examined with data collected over Lake Michigan by Davidson and Safley (1972). Figure 19 includes ramp signatures in temperature traces observed over Lake Michigan where salt accumulation problem would not be a factor. Therefore, the ramp signatures is possibly due to factors associated with the nature of the shear flow itself. On this basis there did not appear to be sufficient evidence to discard data with spikes with ramp signatures. It is not believed that this data being included in this study caused the significant difference between the predicted Wyngaard curve and the observed data curve.

A contradiction occurs between results in Figures 13 and 17. In Figure 13, given the same Z and $\frac{\partial \theta}{\partial z}$ values for both regimes, the plotted curves predict a higher value of C_T^2 for the overwater regime for Ri > -.5 and a higher value of C_T^2 in the overland regime for Ri < -.5. On the other hand in Figure 17, given the same Z and ΔT values for both regimes, the plotted curves predict a higher value of C_T^2 in the overwater regime for X < 1.5 and a higher value of C_T^2 in the overland regime for X > 1.5. Since Ri and X are correlated they should predict basically the same result. However, as is seen in Figures 13 and 17, the only ranges where they correlate is the near neutral range.

In order to explain the reason for this contradiction, values of Ri were plotted versus values of X, Figure 20. The circles show average values of Ri for X intervals of 1.0.

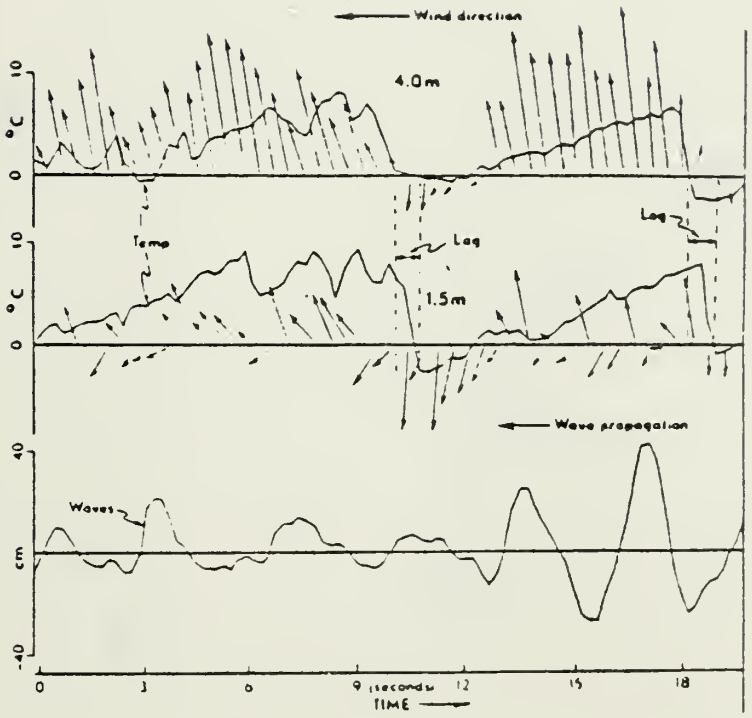

Fig. 19. Temperature trace and velocity fluctuation vectors and wave heights associated with microthermals observed over Lake Michigan.

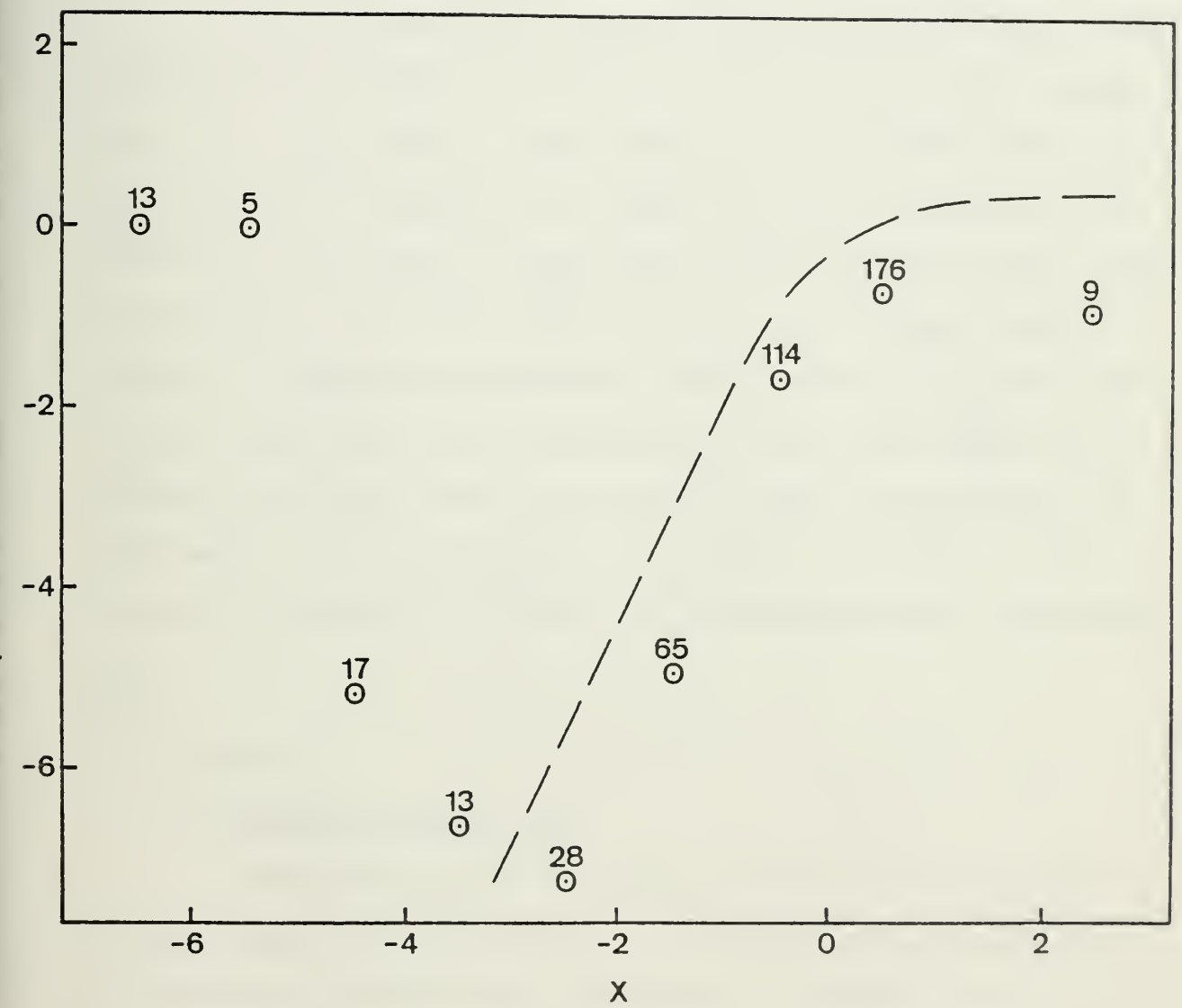

Fig. 20. X versus Richardson number.

Since Z/L is correlated with X, a similar relationship should be seen between X and Ri as exists between Z/L and Ri. The depicted curve is similar to the latter relationship. The conclusion is that the expected correlation existed between these two stability parameters.

A second possible reason for the contradiction is the relationship between $Z^{2/3}/\Delta T^2$ and $1/Z^{4/3}(\partial\theta/\partial z)^2$ which normalize C_T^2 in the DTSFP. Mean values of the former versus the latter appear in Figure 21. There should be a positive correlation between the two and this occurs only for large values of $1/Z^{4/3}(\partial\theta/\partial z)^2$. For small values of the latter there is, however, a negative correlation. This result indicates that the two parameters are correctly correlated when small temperature gradients exist, but are not when the gradients become large. The contradiction is likely to be due to the problem of accurately defining the bulk temperature difference, ΔT.

B. ε RESULTS

1. Gradient Description

Comparison of the observed ε results and the curve based on Equations (23) and (24) is shown in Figure 22 where the predicted curve is the solid line. Averages over Ri intervals of .25 of observed data appear as small circles. The error bars are standard deviations from the mean within each interval. The number of observations defining each mean value is at the top of the error bars. The significant difference between the predicted curve and the observed data

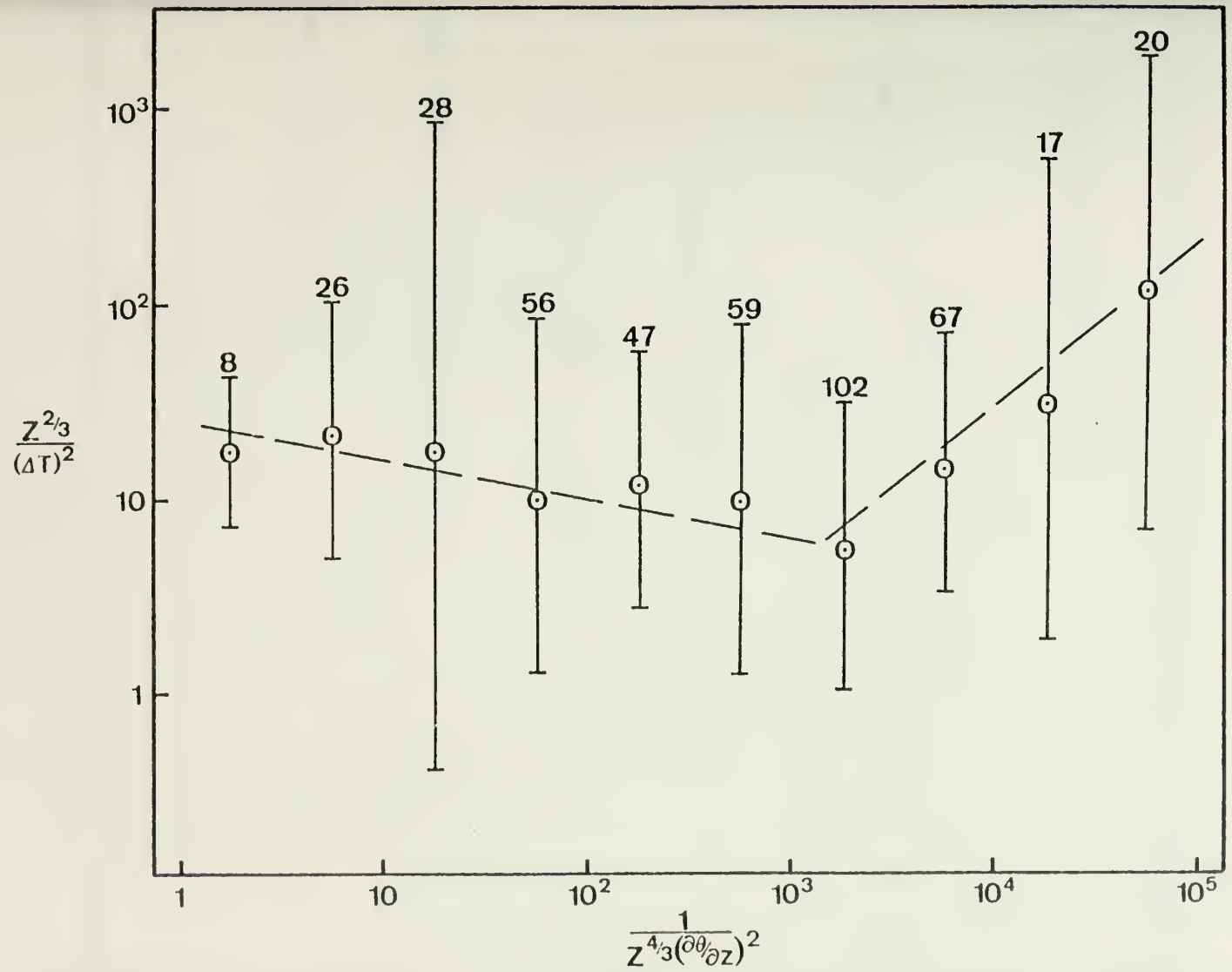

Fig. 21. $\frac{Z^{2/3}}{(\Delta T)^2}$ versus $\frac{1}{Z^{4/3}(\frac{\partial\theta}{\partial Z})^2}$.

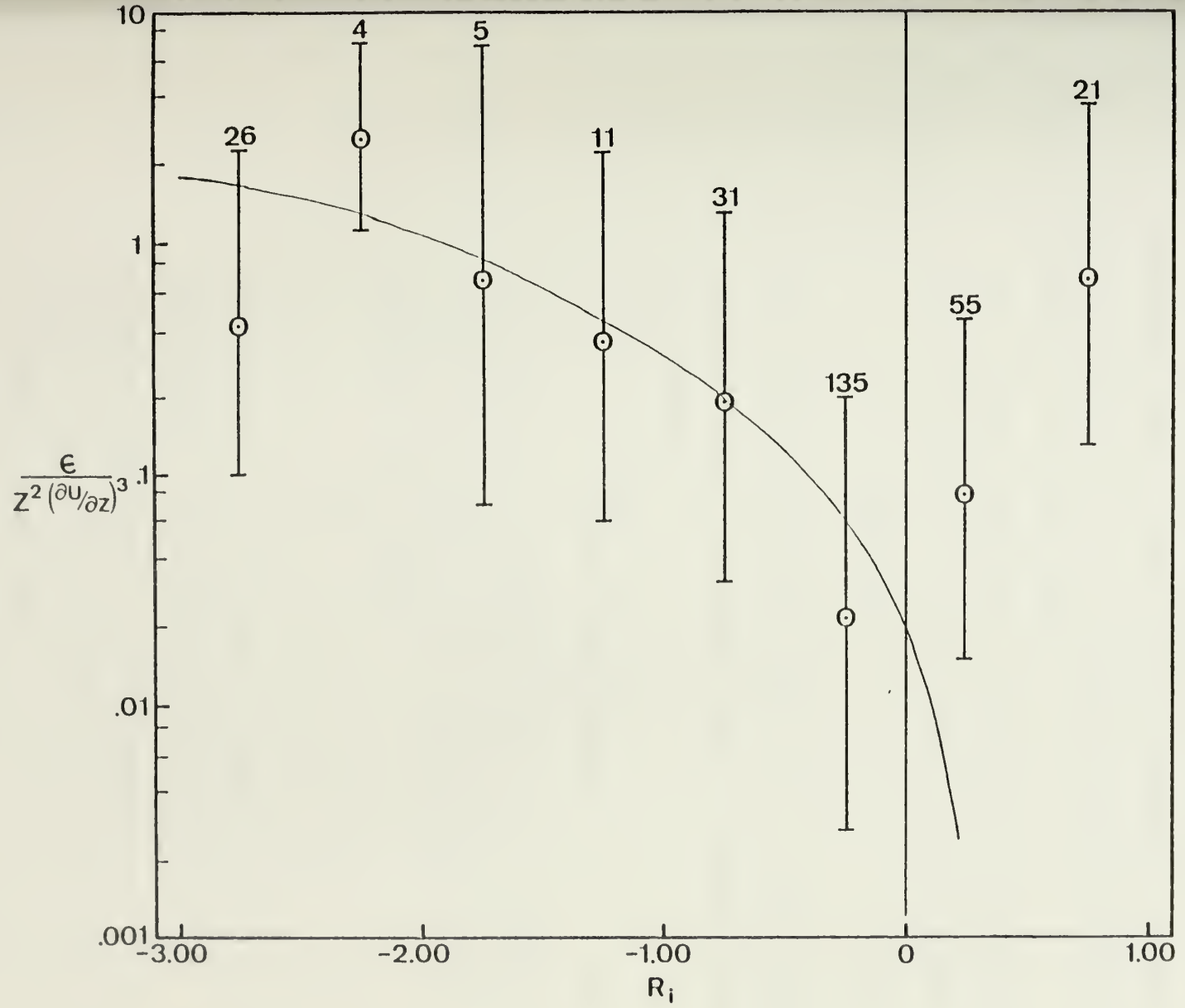

Fig. 22. The dimensionless dissipation rate versus Richardson number.

for Ri > .20 is expected on the basis of Equation (23). For Ri > .20 the equation is no longer valid since terms in the expression become infinite.

An examination of Equations (13), (14), and (15) with the knowledge that U_*^3 and L are independent of height in the surface layer yields the following general prediction for the variation of ε with height:

a. For neutral conditions, (Z/L = 0), ε will decrease with height as Z^{-1} since Equation (15) becomes

$$\varepsilon = \frac{U_*^3}{K} Z^{-1} \qquad (51)$$

b. For stable conditions, (Z/L > 0), ε will decrease less rapidly with height than Z^{-1} since Equation (15) becomes

$$\varepsilon = \frac{U_*^3}{K} Z^{-1}(1+3.7\ Z/L) \qquad (52)$$

c. For unstable conditions, (Z/L < 0), ε will decrease less rapidly with height than Z^{-1} since Equation (15) becomes

$$\varepsilon = \frac{U_*^3}{K} Z^{-1}(1-15\ Z/L)^{-\frac{1}{4}} - Z/L \qquad (53)$$

The quantity in brackets increases with increasing height. This increase is less than for stable conditions. So the decrease of ε with height for unstable conditions is less than that for stable conditions.

Results in Figures 23 and 24 indicate that under near neutral conditions ε fits a Z^{-1} height distribution quite well. There appears to be no change in the height distribution as the surface is approached as there was with C_T^2.

2. Bulk Aerodynamic

Results obtained from analyses with bulk aerodynamic variables appear in Figure 25. The predicted curve is the solid line, while the circles are mean non-dimensional ε results over X intervals of 1.0. Again, standard deviations corresponding to mean values are vertical lines and the number above these lines indicate the number of values defining each mean. The correlation between the non-dimensional ε values versus X, as described for Z/L by Busch and Panofsky (1969), is quite good.

C. C_T^2 RESULTS AT REGIONS ABOVE SURFACE LAYER

A Cessna was used in this experiment to extend the data base beyond the height of the instrumented towers. Height distribution of C_T^2 values as expressed in Equations (46), (47), and (45), have been shown to be valid to height above 4000 meters (Tsvang, 1969). Figure 26 shows that a $Z^{-2/3}$ distribution exists, indicating stable or near neutral conditions, from lowest level to about 100 meters. Above 100 meters, there is a rapid increase of C_T^2 values.

Frisch and Ochs (1975) suggested that if the height of the inversion base, Zi, is another relevant scaling parameter, then proceeding in a manner similar to that of Wyngaard et al,

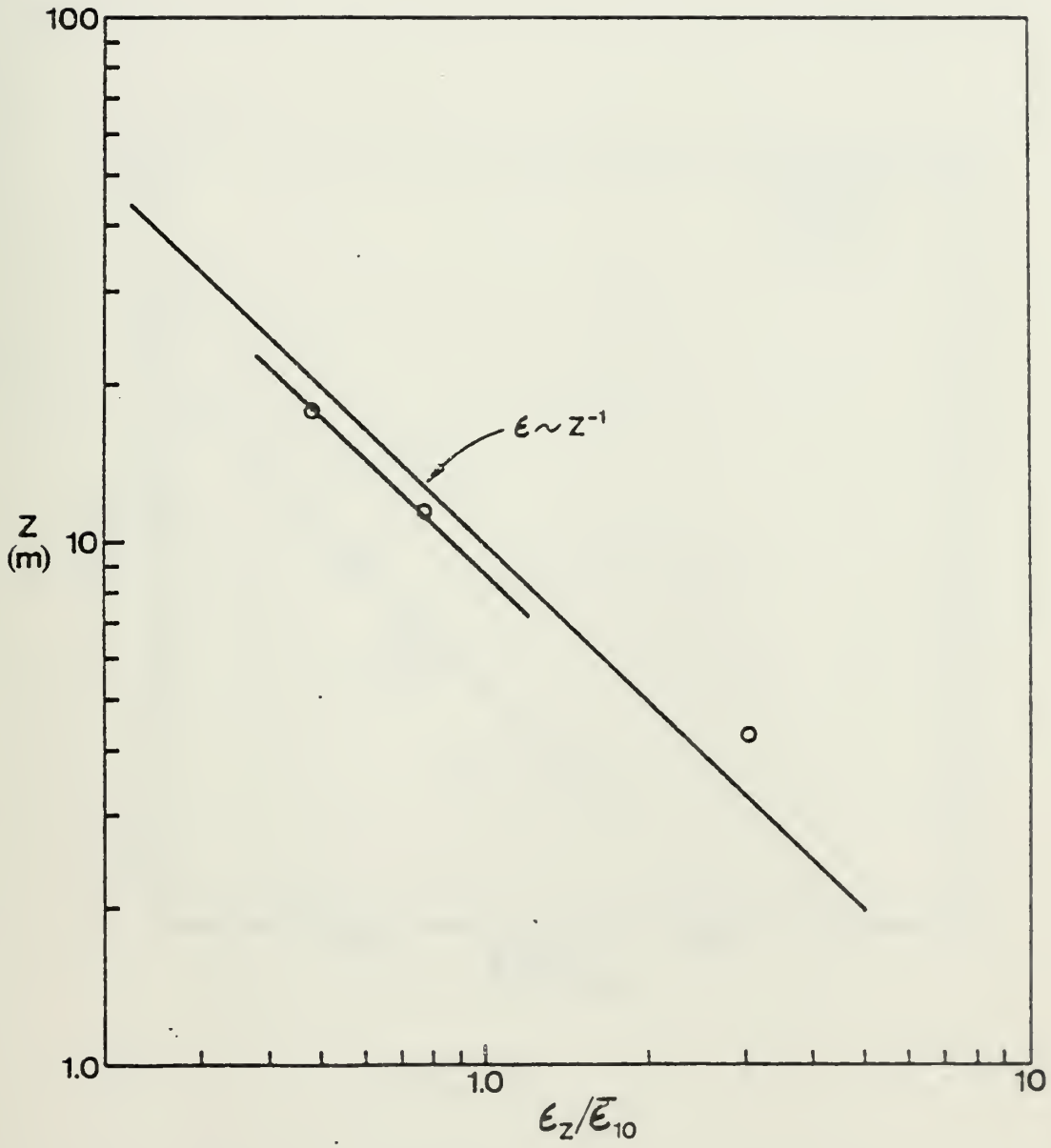

Fig. 23. ε versus log Z.

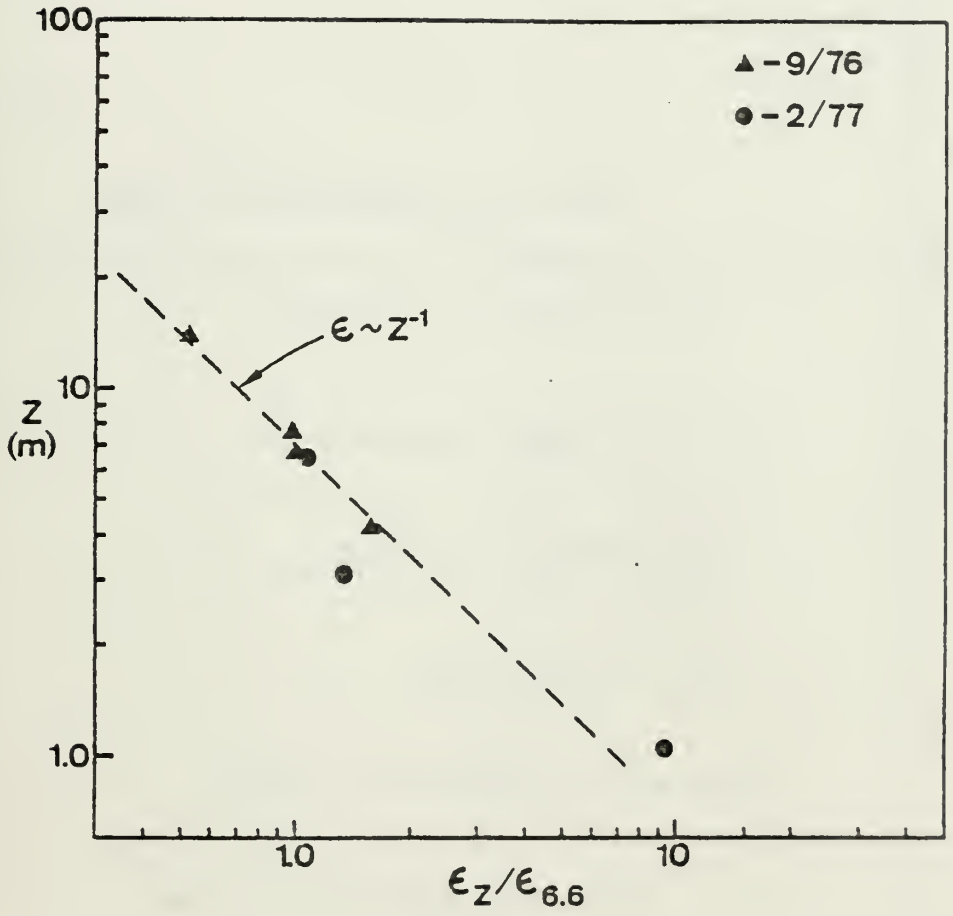

Fig. 24. ε versus log Z.

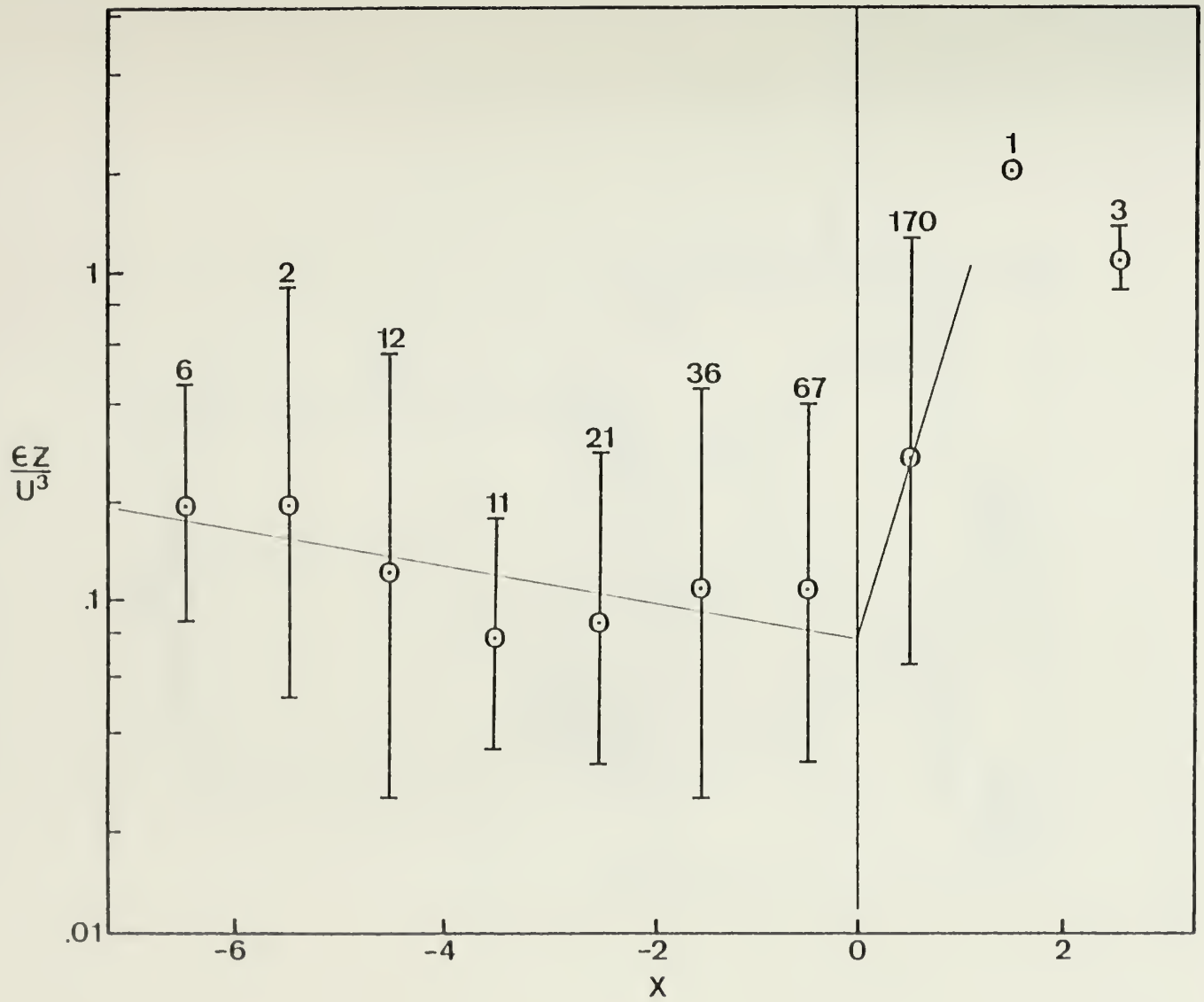

Fig. 25. The dimensionless dissipation rate versus X.

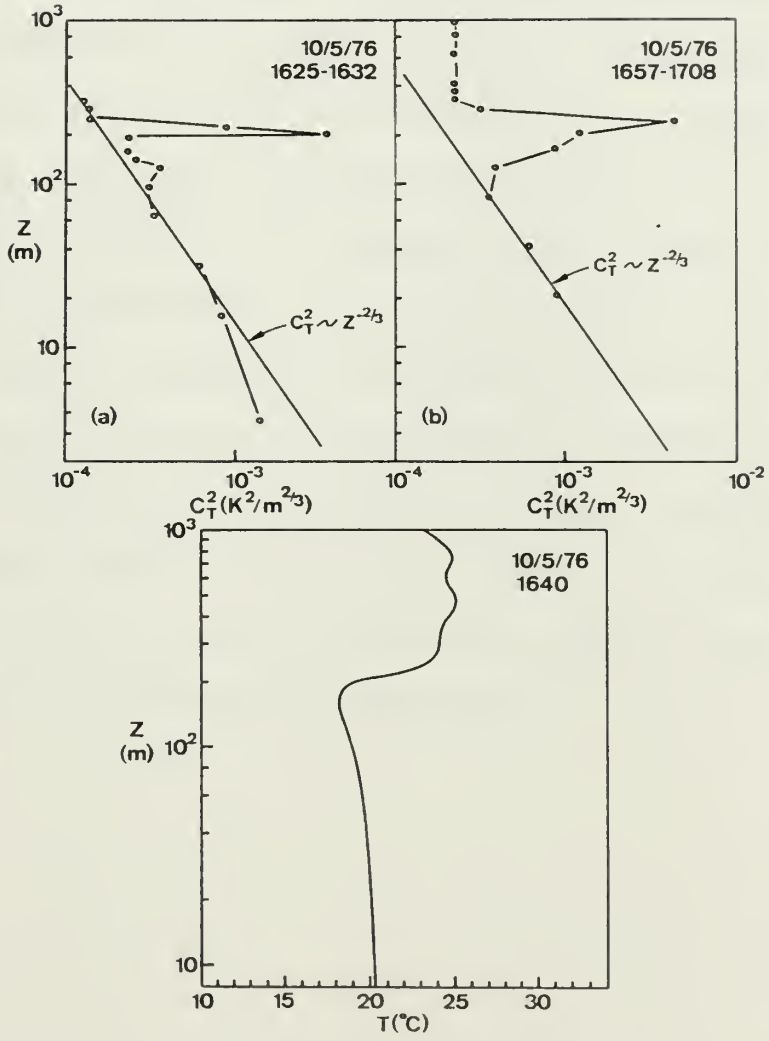

Fig. 26. C_T^2 height distribution and temperature profile.

Equation (47) could be modified with an additional non-dimensional function, $G(Z/Z_i)$. Equation (47) then becomes

$$C_T^2 = \left[\frac{4}{3k^{2/3}}\right](\bar{T}/g)^{2/3}(\overline{w'\theta'})^{4/3}Z^{-4/3}\ G\left(\frac{Z}{Z_i}\right) \quad (54)$$

where $G(Z/Z_i) = 1$ for $Z/Z_i << 1$ in order to have Equation (54) reduce to Equation (47) in the surface layer.

Frisch and Ochs found a significant departure from a $Z^{-4/3}$ law for values of $Z/Z_i > 0.1$. This indicates that the atmosphere is no longer in the "free convection" regime, but is affected by the lid on the convective layer at Z_i. This effect would restrict the integral scale of the turbulent temperature fluctuations with height compared to the free convection value. In addition, because of the layer scale circulation and mixing, the temperature variance should be greater than the free convection variance. These effects will increase the value of C_T^2 relative to the free convection prediction. Figure 26 shows the rapid increase of C_T^2 values as the inversion is approached.

V. CONCLUSIONS

Application of formulated overland expressions in the overwater regime showed a significant difference between observed C_T^2 overwater data and overland predictions. This difference is attributed to the wave influence for near neutral and stable conditions and to the aerodynamic smooth properties of the sea surface during light wind periods for moderate unstable conditions. The formulation of these overwater curves will greatly enhance the Navy's operational ability to describe the marine boundary layer and its influence on the optical wave propagation.

In comparing the DTSFP overland and overwater when plotted against Ri and then versus X, significant differences were noted. Conclusive explanations for this difference cannot be given in this study. Therefore, recommend that serious consideration be given to an in-depth examination of this significant feature.

Correlation of non-dimensional ε values with the stability parameter, Ri, showed agreement between results and predictions. For Ri > .20, the theory is not valid and therefore there was very poor correlation. Any attempt to describe the normalized ε for Ri > .20 in the future will require an expression which will remain valid for all values of Ri.

C_T^2 results appear to be described by the same high distributions up to levels well above the surface layer, approximately 60% of the distance to the marine inversion.

LIST OF REFERENCES

1. Busch, N. E. and Panofsky, H. A., 1968: "Recent Spectra of Atmospheric Turbulence," Q. J. Roy. Meteor. Soc., 94, 132-148.

2. Businger, J. A., Wyngaard, J. C., Izumi, Y., Bradley, E. F., 1971: "Flux Profile Relationship in the Atmospheric Surface Layer," J. Atmos. Sci., 28, 181-188.

3. Corrsin, S., 1951: "On the Spectrum of Isotropic Temperature Fluctuations in an Isotropic Turbulence," J. Appl. Phys., 22, 469-473.

4. Davidson, K. L., Houlihan, T., Schacher, G., and Fairall, C., 1977: "An Examination of Scaling Laws for C_T^2 in the Layer Adjacent to Ocean Waves," Proceedings Topical Meeting on Optical Propagation Through Turbulence, Rain and Fog, Boulder, Colo., 5 pp.

5. Friehe, Carl A., 1976: "Estimation of the Refractive-Index Temperature Structure Parameter over the Ocean," Applied Optics, 16, 334-340.

6. Friehe, Carl A. and Schmitt, Kurt F., 1976: "Parameterization of Air-Sea Interface Fluxes of Sensible Heat and Moisture by the Bulk Aerodynamic Formulas," J. Phys. Oceanogr., 6, 801-807.

7. Garratt, J. R., 1972: "Studies of Turbulence in the Surface Layer over Water (Lough Neagh) Part II. Production and Dissipation of Velocity Fluctuation," Q. J. Roy. Meteor. Soc., 94, 642-657.

8. Houlihan, T., Schacher, G., Fairall, C., Davidson, K., 1977: "Observational Results on Marine Fog Related Variation of Small Scale Turbulence Parameters (C_T^2 and ε)," Proceedings, Topical Meeting on Optical Propagation Through Turbulence, Rain and Fog, Boulder, Colo., 5 pp.

9. Hughes, Michelle Marie, 1976: "An Investigation of Optically Revelant Turbulence Parameters in the Marine Boundary Layer," M. S. Thesis, Naval Postgraduate School, Monterey, Calif., March 1976, 63 pp.

10. Karch, George William, 1976: "An Examination of Turbulent Dissipation in the Marine Boundary Layer," M. S. Thesis, Naval Postgraduate School, Monterey, Calif., December 1976, 72 pp.

11. Kolmogorov, A. N., 1941: The Local Structure of Turbulence in Incompressible Viscous Fluid for Very Large Reynolds Numbers," Doklady ANSSSR, 30, p. 301.

12. Lawrence, R. S., Ochs, G. R., and Clifford, S. F., 1970: "Measurements of Atmospheric Turbulence Relevant to Optical Propagation," J. Opt. Soc. Amer., 60, 826-830.

13. Lumley, J. L., 1973: "Interpretation of Time Spectra Measured in High-Intensity Shear Flows," Phys. of Fluids, 8, 1056, 1060.

14. Monin, A. S., and Obukhov, A. M., 1959: "Basic Laws of Turbulent Mixing in the Ground Layer of the Atmosphere," Akademiia NAVK USSR, Leningrad, Geofizicheskii Institut, Trudy No. 24(151), 163-187, English Translation by Miller, J.

15. Pond, S., Phelps, G. T., and Paquin, J. E., 1971: "Measurements of the Turbulent Fluxes of Momentum, Moisture and Sensible Heat over the Ocean," J. Atmos. Sci., 28, 901-915.

16. Wyngaard, J. C. and Izumi, Y., 1971: "Behavior of the Refractive-Index-Structure Parameter near the Ground," J. Opt. Soc. Amer., 61, 1646-1650.

INITIAL DISTRIBUTION LIST

		No. Copies
1.	Defense Documentation Center Cameron Station Alexandria, Virginia 22314	2
2.	Library, Code 0142 Naval Postgraduate School Monterey, California 93940	2
3.	Department of Meteorology Library Naval Postgraduate School Monterey, California 93940	1
4.	Prof. Kenneth L. Davidson, Code 63Ds Department of Meteorology Naval Postgraduate School Monterey, California 93940	9
5.	Prof. Thomas M. Houlihan, Code 69Hm Department of Mechanical Engineering Naval Postgraduate School Monterey, California 93940	2
6.	Captain Harry Hughes AFIT/CIPF Wright-Patterson AFB, Ohio 45433	2
7.	Lieutenant M. M. Hughes PMS 405 Naval Sea Systems Command Washington, D. C. 20632	3
8.	Captain Alan Simoncic 370A Bergin Monterey, California 93940	1
9.	Captain Valente Macias, Jr. 6439 Louise N.E. Albuquerque, New Mexico 87109	3
10.	Air Weather Service AWS/TF Scott AFB, Illinois 62225	1

Thesis
M18946
c.1

170811

Macias
An investigation of electro-optical turbulence parameters.